



OPEN

Preparation of GaN/Porous silicon heterojunction photodetector by laser deposition technique

Makram A. Fakhri¹, Haneen D. Jabbar¹, Mohammed Jalal AbdulRazzaq¹, Evan T. Salim², Ahmad S. Azzahrani³, Raed Khalid Ibrahim⁴ & Raid A. Ismail²

In this work, gallium nitride (GaN) thin film was deposited on porous silicon (PSi) substrate via a pulsed laser deposition route with a 355 nm laser wavelength, 900 mJ of laser energy, and various substrate temperatures ranging from 200 to 400 °C. The structural and optical properties of GaN films as a function of substrate temperature are investigated. XRD studies reveal that the GaN films deposited on porous silicon are nanocrystalline with a hexagonal wurtzite structure along (002) plane. The photoluminescence emission peaks of the GaN/PSi prepared at 300 °C substrate temperature are located at 368 nm and 728 nm corresponding to energy gap of 3.36 eV and 1.7 eV, respectively. The GaN/PSi heterojunction photodetector prepared at 300 °C exhibits the maximum performance, with a responsivity of 29.03 AW⁻¹, detectivity of 8.6 × 10¹² Jones, and an external quantum efficiency of 97.2% at 370 nm. Similarly, at 575 nm, the responsivity is 19.86 AW⁻¹, detectivity is 8.9 × 10¹² Jones, and the external quantum efficiency is 50.89%. Furthermore, the photodetector prepared at a temperature of 300 °C demonstrates a switching characteristic where the rise time and fall time are measured to be 363 and 711 μs, respectively.

There are numerous uses for ultraviolet photodiodes, including environmental monitoring, optical communication, the detection of missiles, and space exploration^{1–4}. In order to produce a p–n junction photodiode, it is necessary to select a wavelength that minimises the background noise generated by the remainder of the spectrum^{5–8} as well as construct the photodiode's structure from a material that determines its adaptability in severe environments^{9–12}. In modern optoelectronics, the p–n junction photodiode is a fundamental component that is made by combining two semiconductor materials with different bandgaps and other properties, opening the door to novel functionalities and improved overall performance of optoelectronic devices (laser diodes, light-emitting diodes (LED), solar cells, and photodiodes)^{13–18}.

The next generation of photodiodes is expected to exhibit increased light absorption, photo-responsivity, and spectrum sensitivity^{19–22}. As a result, gallium nitride (GaN) stands out as the foundational material for the nitride class of III-nitride semiconductor materials, thanks to its superior thermodynamic stability^{23–25}. GaN is characterized by excellent thermal stability, a small dielectric constant, high thermal conductivity, chemical inertness, radiation hardness, and a wide direct band gap of 3.4 eV^{26–30}. Moreover, GaN possesses exceptional UV photoresponse, well-established mixing techniques, and the capability to operate effectively in high-temperature and challenging environments. Consequently, it finds widespread use in optoelectronic devices that necessitate a layer enabling fast carrier transport and a high breakdown voltage. GaN is particularly utilized in the fabrication of high-power and high-temperature devices operating in the blue and ultraviolet wavelengths^{31–33}.

Pulsed laser deposition (PLD) is capable of producing high-quality GaN thin films at lower growth temperatures compared to other deposition techniques like MOCVD and MBE³⁴. By adjusting laser parameters such as fluence, pulse duration, and distance between target and substrate, stoichiometry of the deposited films can be precisely controlled. Consequently, PLD enables the deposition of GaN films with fewer defects and improved optical and electrical characteristics³⁵. High-power pulsed lasers facilitate high deposition rates, leading to faster GaN film growth. Furthermore, PLD allows for the deposition of GaN thin films on temperature-sensitive substrates like plastics and polymers at low temperatures. It generates a highly focused and confined plume of materials, resulting in reduced contamination during the deposition process^{36,37}. Additionally, the PLD is highly

¹Applied Science Department, University of Technology-Iraq, Baghdad, Iraq. ²Laser and Optoelectronic Engineering Department, University of Technology-Iraq, Baghdad, Iraq. ³Electrical Engineering Department, Northern Border University, Arar, Kingdom of Saudi Arabia. ⁴AlFarahidi University, Baghdad, Iraq. ✉email: mokaram_76@yahoo.com; makram.a.fakhri@uotechnology.edu.iq; evan_tarq@yahoo.com; evan.t.salim@uotechnology.edu.iq; ahmad.azzahrani@nbu.edu.sa

accurate and does not require extensive monitoring since the composition of the film replicates the composition of the target. The background gas pressure has no impact on the passage or absorption of the laser beam in PLD, allowing the same system to be utilized for growing thin film consisting of various materials. This is achieved by adjusting the background gas pressure and positioning different targets under the laser beam³⁸.

Furthermore, PLD has the capability to create layered materials by utilizing a computer-controlled multi-target holder or carousel³⁹. The ablation geometry provides a degree of freedom as the laser energy source is focused outside the vacuum chamber. This allows for rapid transmission of the target material, leading to increased stoichiometry control increase and significantly faster adjustment of the deposition conditions during the initial tuning process. This feature is particularly advantageous when conducting experiments with different target compositions⁴⁰.

Finally, PLD can be performed on silicon, sapphire, and glass⁴¹. Among these options, the Si (silicon) substrates have garnered significant attention from researchers due to several advantages, including their cost-effectiveness, good thermal conductivity, ease of fabrication, and ability to provide uniform carrier injection into the device. However, Si substrates have a notable mismatch in lattice constant with GaN, leading to high defects density and occurrence of cracks^{42,43}. To address this issue, many researchers have explored the deposition of an AlN buffer layer prior to GaN development in order to reduce flaws and cracks in subsequent layers. Nevertheless, the formation of an AlN buffer layer is time-consuming and expensive, and it may impede carrier injection within the nitride structure^{44–46}. The relationship between the substrate type and the piezoelectric field has been reported⁴⁷. The quantum confined Stark effect (QCSE) arises from the piezoelectric field strength in strained GaN quantum wells. This piezoelectric field strength reduces for GaN when it is deposited on a silicon substrate compared to other substrates⁴⁸.

The objective of this research is to fabricate a high-responsivity photodetector in the UV-A region using a PSi (porous silicon) substrate, in contrast to previous studies that utilized Si and Sapphire substrates. Additionally, this manuscript builds upon our previous work on fabricating porous silicon substrates through a photo-electrochemical etching method, assisted by laser, under optimized etching conditions (10 mA/cm² current density and 10 min etching time)^{49,50}.

Furthermore, this manuscript serves as a continuation of our efforts to fabricate GaN/PSi heterojunction photodiodes using the PLD method, exploring different laser wavelengths and energies to identify the optimal growth conditions specifically for a 355 nm laser wavelength and 900 mJ laser energy^{51,52}. In this study, GaN/PSi heterojunction photodiodes were grown using a PLD system at various substrate temperatures (ranging from 200 to 400 °C) with an Nd: YAG laser operating at a wavelength of 355 nm and a laser energy of 900 mJ. The influence of variable substrate temperatures on the structural characteristics, optical properties, morphological and topographical features, as well as the electrical and performance behavior, was investigated.

Experimental

Preparation of PSi Substrate. The present study extends our previous research in which we utilized porous silicon (PSi) as a substrate to fabricate a GaN/PSi heterojunction photodiode under optimal conditions based on the findings of Haneen et al.^{44,49}. The incorporation of a PSi substrate enhances the efficiency of the photodiode through increased surface area and reduced light reflection, resulting in improved light absorption. Furthermore, the porous nature of PSi enables dopant diffusion and the formation of nanostructures, offering opportunities to customize the electronic properties of the material. After establishing the optimal operating conditions, we proceeded to investigate the impact of different laser wavelengths and powers on the deposition process, following the methodology outlined by Haneen et al.^{44,49}. This study focuses on the influence of varying substrate temperatures ranging from 200 to 400 °C during the PLD process for growing GaN on a PSi substrate using a 355 nm, 900 mJ Nd: YAG laser. Moreover, we carefully examined the effects on the structural, topographical, morphological, optical, electrical, and performance properties to identify the most favorable substrate temperature condition for achieving optimal growth of GaN on the PSi substrate.

Mirror-like n-type Si wafers with electrical resistivity of 1–5 mΩ/cm, 500 μm thickness, <100> orientation purchased from University Wafer, Inc, USA were used. The wafers were then cut into rectangular pieces measuring 1 by 1 cm. Prior to the photo-electrochemical etching process, the pieces were thoroughly cleaned using an ultrasonic device in ethanol (99.9% concentration, Germen, Honeywell company) for a duration of 5 min. The etching process took place at room temperature and involved the use of a diode laser (660 nm, 100 mW, China, Tongtool Company), a DC power supply ranging from 0 to 30 V (China, Jiuyuan), and a digital multi-meter (China, Victor). This process, as illustrated in Fig. 1, necessitates the utilization of a Teflon cell equipped with a cathode electrode composed of 95% pure platinum and an anode electrode made of silicon. The laser was an integral part of the top-down electrochemical etching procedure employed to synthesize the PSi substrates. Furthermore, the etching conditions were carefully regulated, with the etching time set at 10 min, the current density maintained at 10 mA/cm², and the concentration of hydrofluoric acid (HF) (obtained from Germen, Thomas Baker company) in the process consistently maintained at 24% using the dilution formula described in Eq. (1)^{53–55}.

$$C_1V_1 = C_2V_2 \quad (1)$$

where 1 : Hydrofluoric acid concentration, V₁ : Hydrofluoric acid volume, C₂ : Ethanol concentration., V₂ : Ethanol volume.

Following the photo-electrochemical etching process, all prepared PSi substrates underwent a series of tests and experiments to determine the optimal etching parameters, including current densities and etching times^{42,44}. X-ray diffraction analysis was conducted using CuKα radiation with a wavelength of 1.54060 Å using XRD diffractometer (XRD6000, Shimadzu) to investigate the structural properties of the deposited films. Morphological

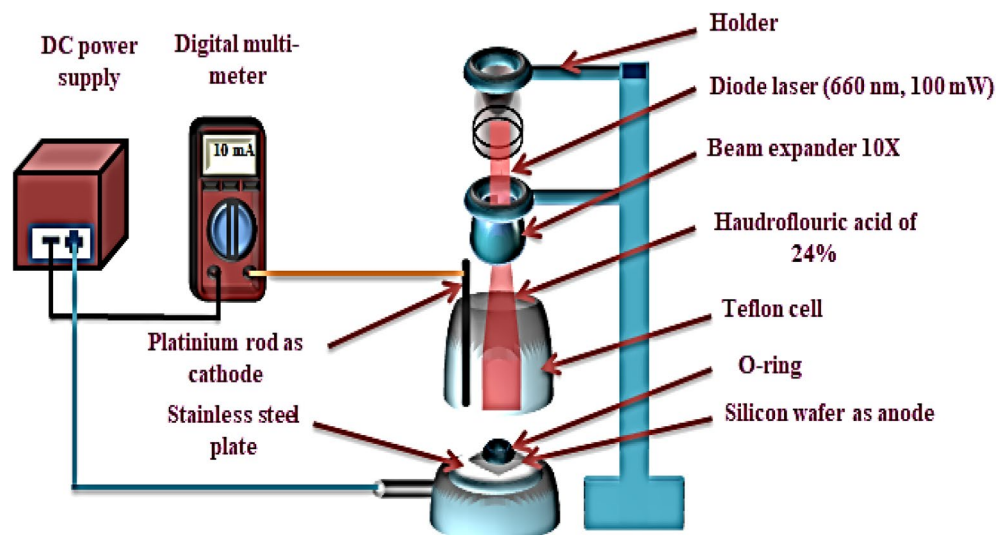


Figure 1. Schematic diagram of Photoelectrochemical etching method assisted by a diode laser under optimum etching conditions⁴².

parameters were measured using a high-resolution German field emission scanning electron microscope (FESEM) from ZEISS Company. The top layer was examined using an AFM (Atomic Force Microscope) (TT-2 Workshop Compan, USA). The photoluminescence (PL) properties of the film are investigated using spectrophotometer (PerkinElmer). The Hall effect measurements (Irasol, Hall Effect measurement system, HSR-25AC) were conducted using to estimate the conduction type of GaN. The results showed that the Hall coefficient of the film was positive indicates that the deposited film is p-type.

Preparation of gallium nitride films. To deposit GaN films using PLD, a high-purity gallium nitride powder with a 99.9% purity level, supplied by Luoyang Advanced Material Corporation, China, was utilized. The powder was pressed using a hydraulic press at a pressure of 15 kg/cm² to form a circular-shaped GaN target weighing 5 g, with a thickness of 0.5 cm and a diameter of 2 cm. Subsequently, the pressed GaN target was ablated using a Q-switching Nd:YAG laser (RY 280, China) operating at an ambient pressure of 10⁻² mbar. The laser had an energy of 900 mJ, a wavelength of 355 nm, and a pulse duration of 7 ns, as shown in Table 1. The most favorable outcomes were achieved by depositing GaN material onto the prepared PSi substrate under optimal growth conditions, as illustrated in Fig. 2.

After the pulsed laser deposition procedure, the synthesized PSi layer and the fabricated GaN nanostructure are characterized.

Electrical properties of GaN/PSi heterojunction. To establish an ohmic contact, as depicted in Fig. 3, an aluminum mask designed in the shape of a fingerprint was carefully positioned over the fabricated GaN/PSi nanostructure. This mask served the purpose of protecting the nanostructure and preserving its performance. Current–voltage characteristics were measured for both the prepared PSi substrate and the fabricated GaN thin film. This was accomplished using a power supply (Dazheng 30V, 5 A PS-305D from China) and digital multimeters (UNI-T-UT33C) in the dark, with forward and reverse bias configurations, respectively (TEKR. CDM 250). Additionally, the capacitance–voltage characteristics were studied by using a programmable LCR meter (GW Instek LCR-6100 from Taiwan) in the frequency range of 10 Hz–100 kHz.

Growth conditions	The values
Laser wavelength	355 nm
Pulse energy	900 mJ
Pulse duration	7 ns
Frequency	3 Hz
Repetition rate	300 Hz
Power supply	220 V
Substrate substrate temperature	Psi 200–400 °C

Table 1. Growth conditions of Nd: YAG laser deposition system.

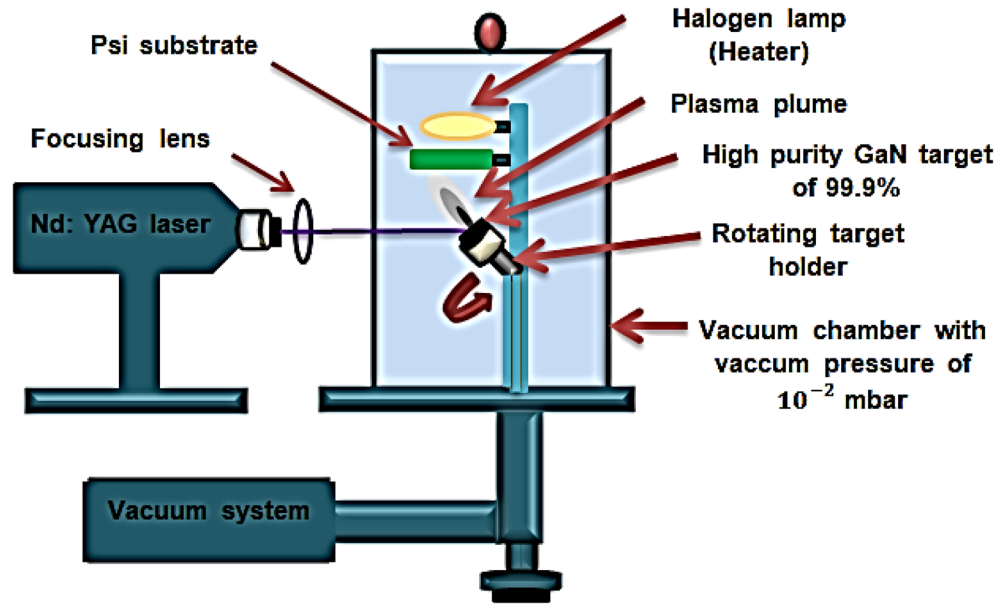


Figure 2. Schematic diagram GaN deposited on PSi substrate using PLD method at different substrate temperatures from 200 to 400 °C¹².

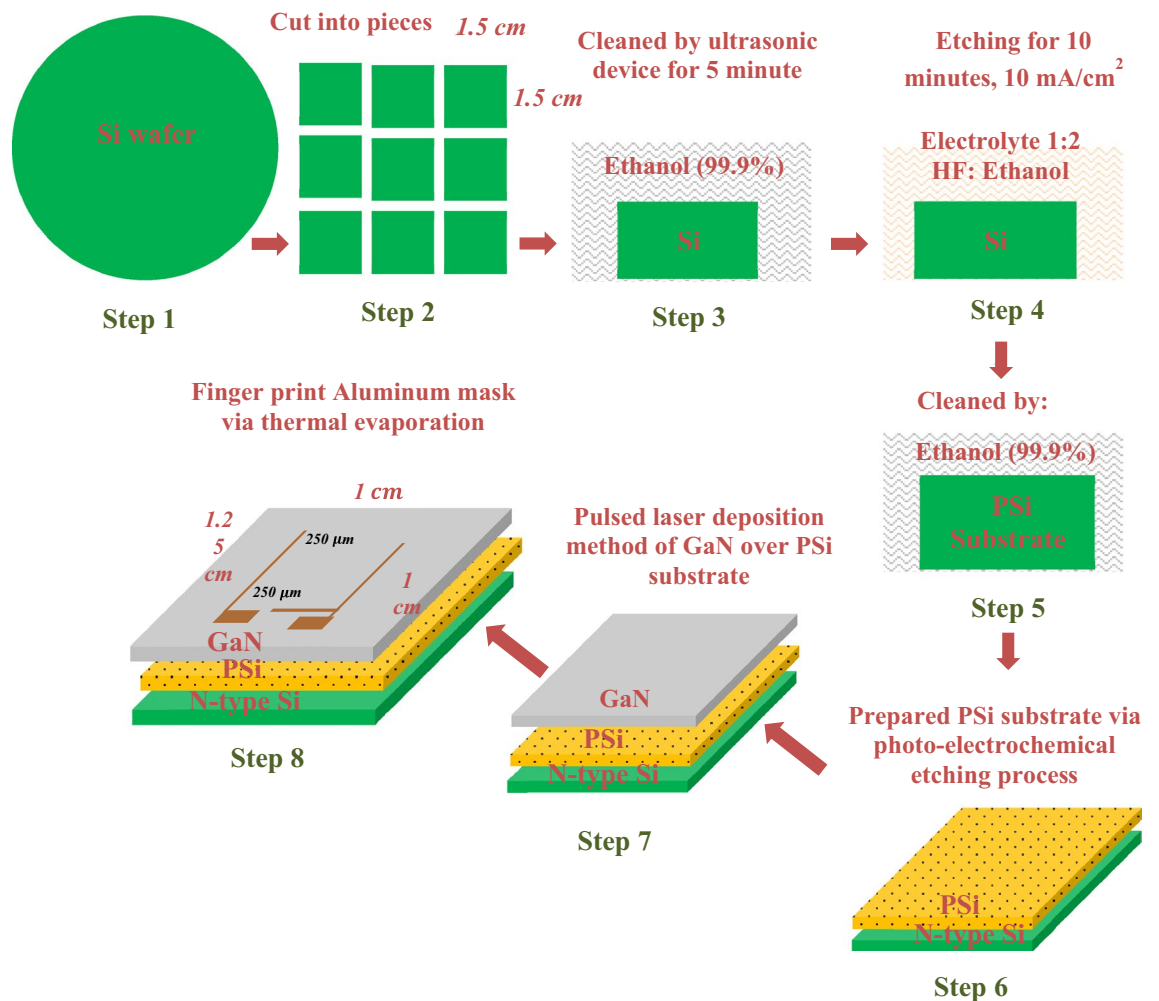


Figure 3. Schematic diagram of preparing GaN/PSi nanostructure using the PLD method.

Results and discussion

Structural properties (XRD). *XRD of PSi substrate.* The XRD patterns of the synthesized PSi substrate, obtained under the optimal working conditions of 10 mA/cm² current density, 10 min etching time, and 24% HF acid concentration, are presented in Fig. 4a. The corresponding analysis of the patterns is provided in Table 2. This figure confirms the presence of XRD peaks associated with both porous silicon and crystalline silicon, which indicates the successful formation of porous silicon. The peaks corresponding to porous silicon are observed at $2\theta = 33^\circ$ and 69° , corresponding to the (200) and (400) crystallographic planes, respectively. As observed, the high intensity peak (400) is splatted into two peaks, one for the Si layer and the other for the PSi layer. As well as, the energy dispersive X-ray (EDX) analysis image confirms existence of O (at 0.5 keV) and Si (at 1.7 keV) as two main peaks to confirm the composition of a produced PSi substrate using aided by a diode laser as shown in Fig. 4b.

XRD of GaN/PSi nanostructures. Figure 5 displays the XRD patterns of the GaN/PSi nanostructures fabricated at various substrate temperatures ranging from 200 to 400 °C. The observed peaks along (100), (002), (101), (110), and (103) planes are indexed to GaN (card # 01-074-0243)⁵². The GaN/PSi nanostructures fabricated at 200 °C exhibited a small peak with a narrow full width at half maximum. As the substrate temperatures increased from 200 to 400 °C, both the peak intensity and the full width at half maximum demonstrated gradual changes. Additionally, according to the data presented in Table 3, films deposited at temperatures above 300 °C exhibited a decrease in crystalline quality, attributed to the formation of structural defects.

The XRD analysis of PSi substrate and GaN film is shown in Tables 2 and 3, respectively. The average crystallite size (D) was calculated using Scherrer's formula^{56–58}, as shown in Eq. (2). The interplanar distance (d) was calculated using the formula as shown in Eq. (3)^{59–61}.

$$D = K\lambda/\beta \cos \theta \quad (2)$$

$$d = n\lambda/2 \sin \theta \quad (3)$$

where $K = 0.9$, λ is the X-ray wavelength, β is the fullwidth at half maximum, θ is the diffraction angle, and n is a represented positive integer.

As well as, the Williamson-Hall method were used to determined the average crystallite size and strain of fabricated GaN over porous silicon nanostructure as listed in Table 4 and as calculated using Eq. (4)^{62,63}.

$$\beta_T \cos \theta = \varepsilon(4 \sin \theta) + \frac{K\lambda}{D} \quad (4)$$

where β is total full width at half maximum, ε is strain, θ is diffraction angle, k is 0.94, λ is the wavelength, and D is the crystallite size.

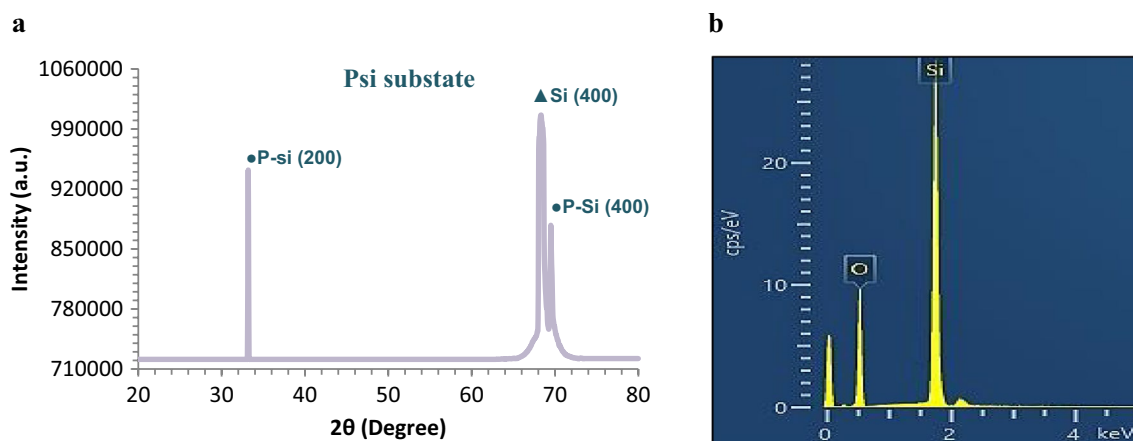


Figure 4. (a) XRD patterns of PSi substrate under optimal etching parameters and (b) EDX of synthesized PSi substrate under optimum etching parameters.

Substrate (PSi) orientation (hkl)	2θ (Degree)	B (Degree)	D (nm)	d (nm)
200	33	0.28	0.27	0.20
400	69.23	0.31	0.13	0.13

Table 2. XRD analysis of PSi substrate^{42,43}.

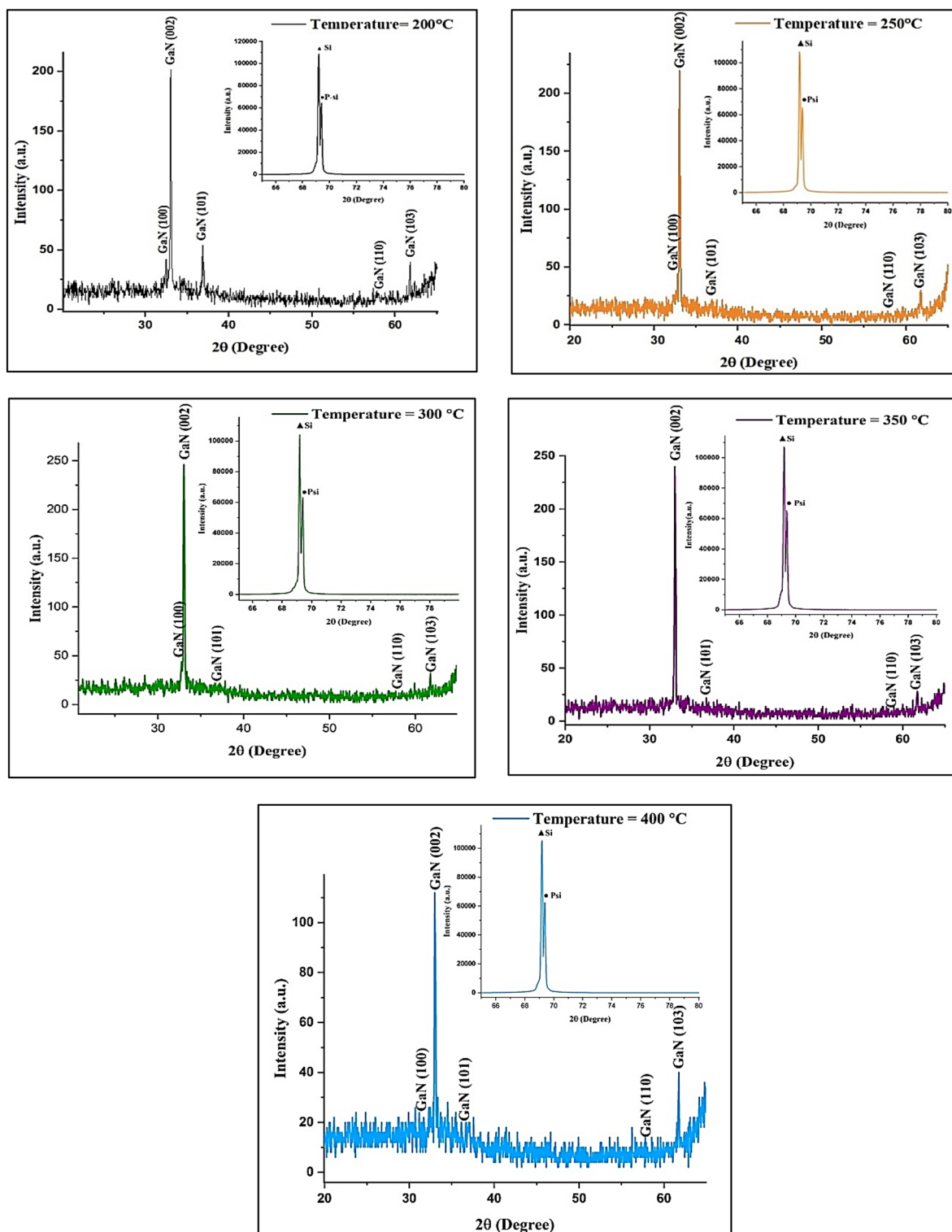


Figure 5. XRD pattern of GaN/Psi nanostructures prepared at various substrate temperatures.

Raman spectroscopy (RS). *RS of PSi substrate.* Figure 6 depicts the Raman spectrum of prepared PSi substrate by photo-electrochemical etching (PECE). One of the main Raman peaks observed in porous silicon is called “Stokes peak” or the “transverse optical (TO) peak,” which is located around $520\text{--}560\text{ cm}^{-1}$. This peak corresponds to the longitudinal optical (LO) phonon mode in crystalline silicon and is shifted to lower frequencies due to the confinement effects in the nanoporous structure^{49,64}.

Substrate temperature (°C)	GaN films orientation (hkl)	2 θ (Degree)	β (Degree)	D (nm)	d (nm)
200	- 100	32.4	0.18	46.01	0.27
	- 2	33	0.15	55.30	0.27
	- 101	36.84	0.21	39.92	0.24
	- 110	57.7	0.58	15.65	0.15
	- 103	61.7	0.17	54.50	0.15
250	- 100	32.7	0.20	41.44	0.27
	- 2	33	0.13	63.81	0.27
	- 101	36.8	0.42	19.95	0.24
	- 110	57.8	0.24	37.85	0.15
	- 103	61.7	0.23	40.28	0.15
300	- 100	32.76	0.20	41.45	0.27
	- 2	33.04	0.18	46.09	0.27
	- 101	36.64	0.44	19.04	0.24
	- 110	57.72	0.08	113.53	0.15
	- 103	61.76	0.14	66.20	0.15
350	- 2	33	0.18	46.08	0.27
	- 101	36.72	0.18	46.56	0.24
	- 110	57.8	0.16	56.78	0.15
	- 103	61.72	0.22	42.12	0.15
400	- 100	32.48	0.28	29.50	0.27
	- 2	33	0.19	43.66	0.27
	- 101	36.8	0.04	209.57	0.24
	- 110	57.8	0.04	227.15	0.15
	- 103	61.76	0.14	66.20	0.15

Table 3. XRD analysis of the GaN/PSi nanocrystalline prepared at various substrate temperatures.

Substrate temperature (°C)	2 θ (Degree)	β_T (Degree)	$\beta_T \cos\theta$	4sin θ	Average crystallite size (nm)	Strain
200	32.4	0.18	0.0030	1.1159	24.4	0.00765
	33	0.15	0.0025	1.1360		
	36.84	0.21	0.0034	1.2639		
	57.7	0.58	0.0088	1.9300		
	61.7	0.17	0.0025	2.0511		
250	32.7	0.20	0.0033	1.1260	38	1.84E-04
	33	0.13	0.0021	1.1360		
	36.8	0.42	0.0069	1.2625		
	57.8	0.24	0.0036	1.9331		
	61.7	0.23	0.0034	2.0511		
300	32.76	0.20	0.00335	1.1280	17	0.00352
	33.04	0.18	0.00301	1.1374		
	36.64	0.44	0.00729	1.2572		
	57.72	0.08	0.00122	1.9306		
	61.76	0.14	0.0021	2.0529		
350	33	0.18	0.0030	1.1360	47	8.04E-05
	36.72	0.18	0.0029	1.2599		
	57.8	0.16	0.0024	1.9331		
	61.72	0.22	0.0032	2.0517		
400	32.48	0.28	0.0046	1.1186	27	0.00204
	33	0.19	0.0031	1.1360		
	36.8	0.04	0.00064	1.2625		
	57.8	0.04	0.00061	1.9331		
	61.76	0.14	0.0020	2.0529		

Table 4. Williamson- Hall analysis of the GaN/PSi nanocrystalline prepared at various substrate temperatures.

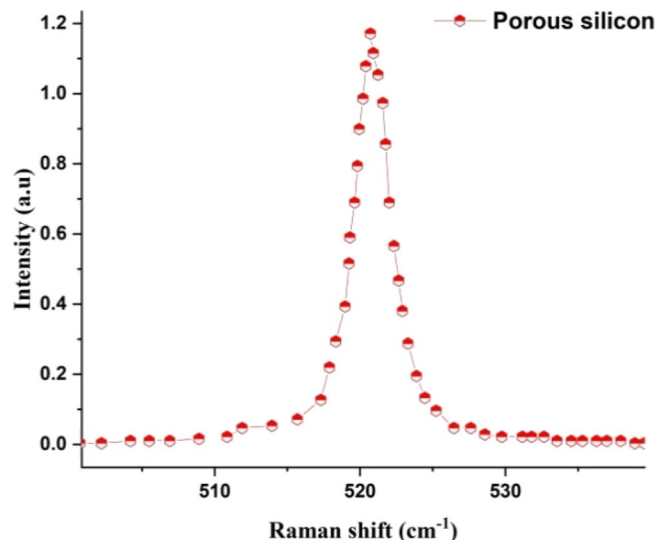


Figure 6. Raman spectra of prepared porous silicon substrate using PECE process assisted by a diode laser under optimum conditions.

RS of GaN/PSi Nano-structures. Figure 7 display Raman spectrum of prepared GaN on PSi nano-structure using PLD method under 900 mJ laser energy, 355 nm laser wavelength, and optimum substrate temperature of 200 °C. Several distinct peaks (775.9, 1141.9, and 1440.9) can be seen in the typical Raman spectra of GaN. The E2 (high) mode is the dominant peak because it is associated with the motion of nitrogen atoms in the crystal lattice. Its location and strength can shed light on the crystal quality and strain of the film they are observing. Additional information about the material can be gleaned from the positions and intensities of other peaks, such as the A1 (TO) and E1 (TO) modes^{49,65}.

Spectroscopic properties. *PL of PSi substrate.* The photoluminescence (PL) spectra of the PSi substrate are presented in Fig. 8. PL measurements of the PSi substrate were conducted at room temperature, with an excitation wavelength of 280 nm. Firstly, it is observed that the prepared PSi substrate exhibits a visible yellow band (589 nm) due to surface states and quantum confinement that arise during the photo-electrochemical etching process, as mentioned by Wang⁶³. Subsequently, utilizing Eq. (5)^{64–66}, the energy band gap of the prepared PSi substrate was determined to be 2.10 eV, which is larger than the energy band gap of silicon (1.11 eV). This difference in energy band gaps can be attributed to the combined effects of quantum confinement and increased

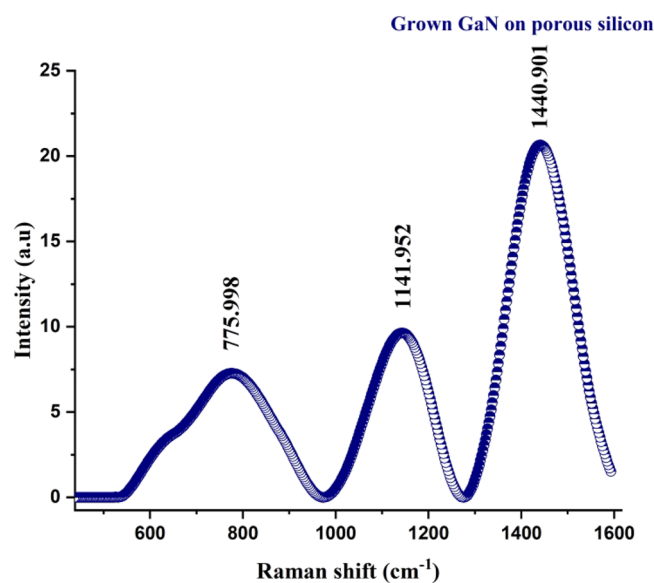


Figure 7. Raman spectrum of prepared GaN on PSi nano-structure using PLD method under 900 mJ laser energy, 355 nm laser wavelength, and optimum substrate temperature of 300 °C.

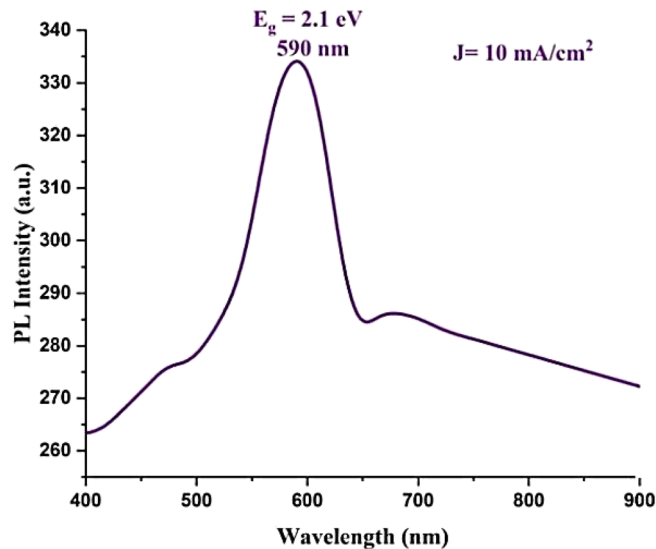


Figure 8. Room temperature PL spectrum of prepared PSi substrate⁴².

surface states, which alter the electronic structure of the material and result in a broader energy gap, as discussed by Canham et al.^{67–69}.

$$E_{\text{gap}} = \frac{hc}{\lambda} = \frac{1240}{\lambda(\text{nm})} \quad (5)$$

where E_{gap} is prepared PSi substrate's energy band gap. h is 6.62×10^{-34} J/s that represent plank's constant. c is 3×10^8 m/s that represent light speed. λ is PSi's wavelength peak (589 nm).

PL of GaN/Psi nano-structures. Figure 9 illustrates the photoluminescence (PL) spectra of GaN nanofilms fabricated at various substrate temperatures ranging from 200 to 400 °C. The PL measurements were conducted on GaN/PSi nanocrystalline films at room temperature, using an excitation wavelength of 320 nm. The results revealed that the GaN nanofilms emitted UV bands corresponding to the characteristic emissions of GaN material, observed at wavelengths of 359.4, 366, 368, 370.7, and 360 nm. Additionally, red bands indicative of the PSi substrate were detected at wavelengths of 722.5, 729, 728, 723.7, and 720.1 nm.

With increasing temperature from 200 to 400 °C, several factors contribute to the observed enhancement in photoluminescence (PL) intensity and reflectance of the GaN film. One of these factors is improved crystal quality, where higher substrate temperatures promote better growth of the GaN film with a more crystalline structure. The elevated temperatures provide greater thermal energy, enabling atoms to move more freely and facilitating the formation of a more orderly crystal lattice. This improved crystal quality results in fewer defects and dislocations, which are known to dampen the photoluminescence (PL) intensity. As a result, the PL intensity of the GaN film increases as the temperature rises. Additionally, the strain is reduced. Temperature influences

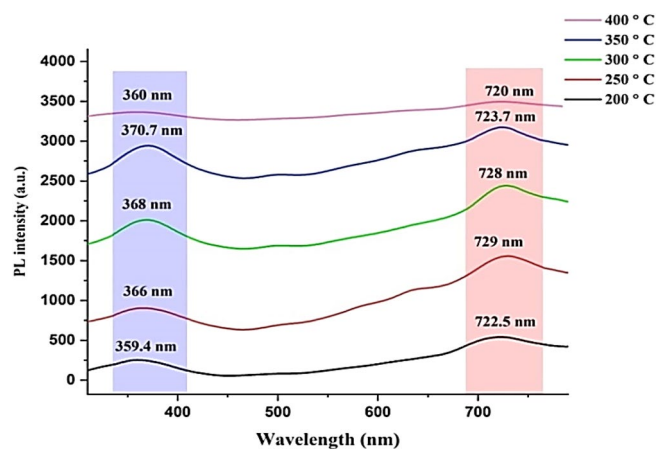


Figure 9. Room temperature PL spectra of GaN/PSi nanostructures prepared at various substrate temperatures.

the lattice matching and strain between the GaN film and the porous silicon substrate. Higher temperatures aid in minimizing the lattice mismatch and strain between the two materials, leading to a lower density of structural defects and dislocations in the GaN film. These defects can function as non-radiative recombination centers, thereby reducing the photoluminescence (PL) intensity. Consequently, by elevating the substrate temperature, the strain is alleviated, resulting in an increase in PL intensity. Furthermore, there is an improvement in surface morphology. The temperature of the substrate also impacts the surface morphology of the GaN film. Higher temperatures during the deposition process facilitate surface diffusion and lead to the smoothing of the film. A smoother surface reduces scattering and enhances light extraction efficiency, resulting in increased reflectance. The enhanced reflectance contributes to higher PL intensity as more emitted photons are reflected back, increasing the likelihood of their detection^{70–73}.

Diffused reflected spectroscopy (DRS). *DRS of PSi substrate.* Diffused reflectance spectroscopy was conducted on the synthesized PSi. The measurements were performed in the spectral range from 230 to 1000 nm, as depicted in Fig. 10. Additionally, as shown in Fig. 11, the energy bandgap of the synthesized substrate was determined by calculating the absorption spectra derived from the diffuse reflectance using the Kubelka–Munk function $F(R)$. The calculation was carried out using the following Equation^{74–76}:

$$F_{(k-m)} = \frac{(1 - R^2)}{2R} \quad (6)$$

where F_{K-M} is Kubelka–Munk function, and R is the reflectance obtained from diffused reflected spectroscopy.

DRS of GaN/Psi nano-structures. The diffused reflectance spectroscopy of the fabricated GaN/PSi nanostructure, prepared using the PLD method at various substrate temperatures ranging from 200 to 400 °C, was measured and is depicted in Fig. 12. Furthermore, Fig. 13 illustrates the energy bandgap, which was calculated from the absorption spectra derived from the diffuse reflectance using the Kubelka–Munk function $F(R)$ with the help of Eq. (5)^{74–76}. Notably, at a substrate temperature of 300 °C, the fabricated GaN/PSi nanostructure exhibits significantly higher reflectance in the UV region spectrum compared to other substrate temperatures. As the substrate temperature is increased in the PLD method, several factors contribute to the increased reflectance. One of these factors is improved crystallinity. The elevation of substrate temperature during PLD promotes the growth of a more crystalline GaN film. This higher degree of crystallinity leads to a smoother film surface with fewer defects, resulting in reduced light scattering and increased reflectance. In addition, higher temperatures can enhance the adhesion between the GaN film and the substrate. This improved adhesion minimizes the presence of interfacial gaps and irregularities, thereby leading to improved reflection properties. Moreover, increasing the temperature can also result in a reduction in porosity. Porous silicon substrates typically possess high porosity, which can cause light to scatter and be absorbed within the substrate. By raising the temperature, thermal annealing of the porous silicon occurs, leading to a decrease in porosity. Consequently, more light is reflected off the GaN film rather than being absorbed or scattered within the substrate. Furthermore, elevated temperatures can contribute to a reduction in surface roughness. This is achieved through surface diffusion processes promoted by the increased temperature, resulting in the smoothening of the GaN film surface. A smoother surface reduces light scattering and enhances reflectance^{37,77,78}.

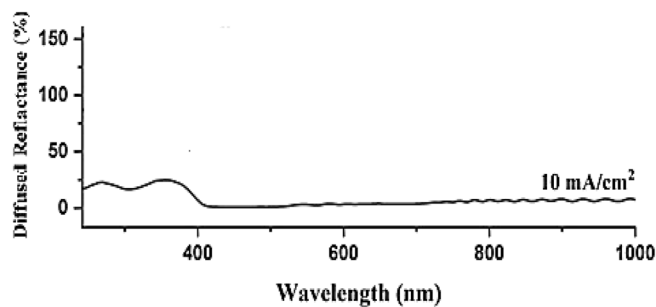


Figure 10. Surface reflectance of PSi substrate.

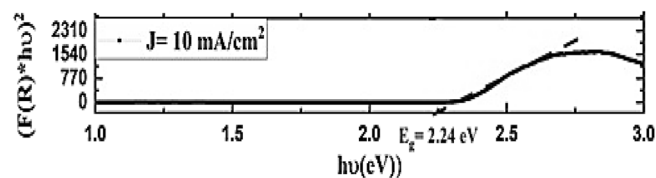


Figure 11. Synthesised PSi substrates Kubelka Munk function.

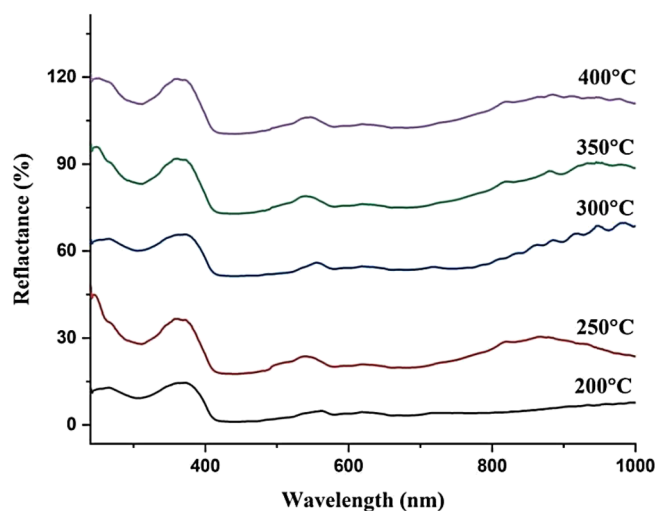


Figure 12. Reflectance of GaN/PSi nanostructures made by the PLD process at substrate temperatures between 200 and 400 °C.

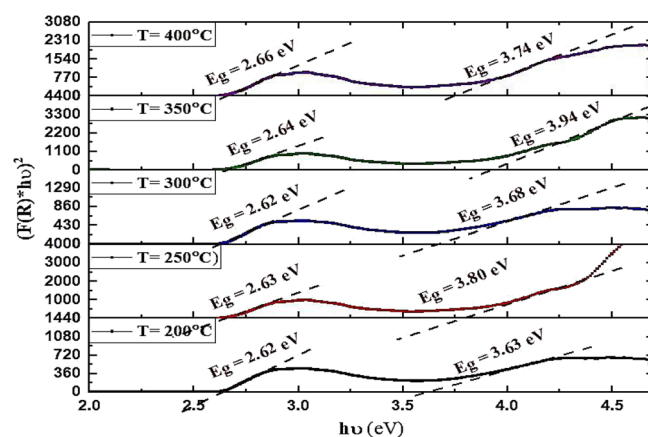


Figure 13. Kubelka–Munk function of GaN/PSi nanostructures made by the PLD process at substrate temperatures between 200 and 400 °C.

Surface topography AFM. *AFM of PSi substrate.* Figures 14a,b present an AFM image and the distribution of grain sizes, respectively, for a prepared PSi substrate that underwent laser-assisted photo-electrochemical etching to investigate surface topography. Upon etching for 10 min, uniformly distributed pores formed across the entire surface, exhibiting an elongated oval shape. The AFM parameters of the prepared PSi substrate are provided in Table 5. Notably, nanometer-scale analysis was conducted to determine the particle size distribution of the PSi substrate after preparation.

AFM of GaN/PSi Nano-structures. Figure 15 shows three-dimensional AFM images and the size distribution of the grains in GaN nanofilms fabricated at different substrate temperatures. As shown in Table 6, increasing the substrate temperature from 200 to 400 °C resulted in smoother surfaces and reduced surface roughness, with the lowest roughness observed at a substrate temperature of 400 °C. The researchers attributed the improvement in surface morphology to the increased mobility of the GaN adatoms at higher substrate temperatures^{79,80}.

Surface morphology FESEM. *FESEM of PSi substrate.* Figures 16a,b display FE-SEM images of the surface and cross-section, respectively, of the PSi substrates, providing insight into the surface morphology.

Consistent with the findings of Omar et al.⁵¹, the surface pores exhibit a star-like appearance and maintain a consistent elongated shape across the entire surface. This characteristic appearance is attributed to the utilization of low-resistance n-type silicon (100) during the preparation process. Additionally, the thickness of the PSi layer was determined to be 36.02 nm based on a cross-sectional FE-SEM image^{43,81}.

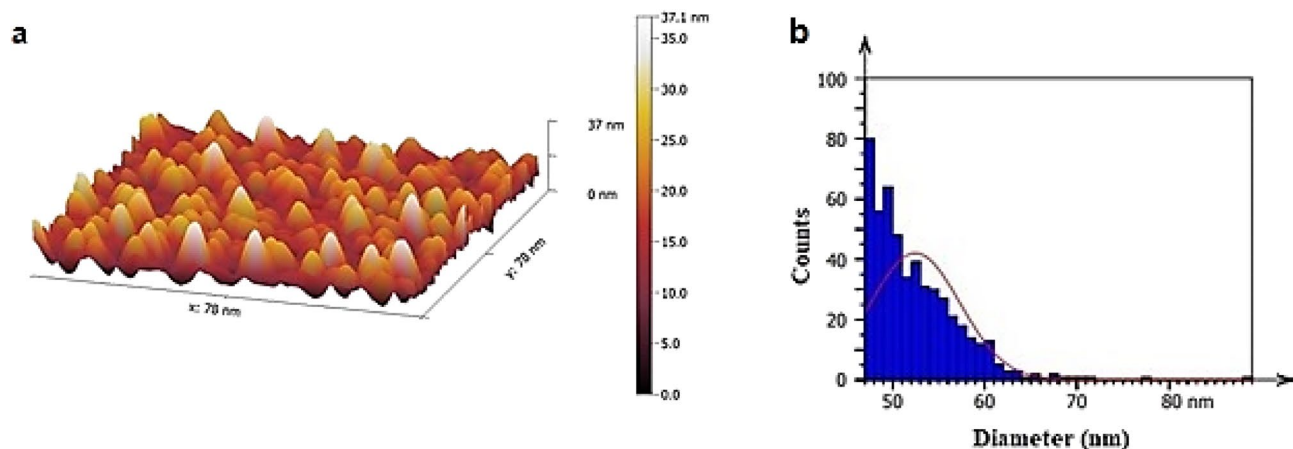


Figure 14. (a) AFM image of prepared PSi substrate; (b) grain size distribution image of prepared PSi substrate^{42,43}.

Root-mean-square height (nm)	Maximum height (nm)	Average surface roughness (nm)	Average diameter (nm)
11.88	37	9.40	52.46

Table 5. AFM parameters of synthesized PSi substrate^{42,43}.

FESEM of GaN/PSi nano-structures. Figure 17 depicts FE-SEM images of GaN/PSi nanostructures fabricated using the PLD method, highlighting the influence of varying substrate temperatures ranging from 200 to 400. Microscopy and nanotechnology techniques were utilized to examine the surface morphology of the GaN films. The resulting GaN nanoparticles completely covered the PSi substrate, forming spherical particles of uniform and homogeneous size, resembling the shape of cauliflower. Additionally, the cross-section of the GaN nano-films was examined using FE-SEM to determine their thickness as listed in Table 7. It was observed that the substrate temperature had a significant impact on the surface morphology of the GaN thin films grown through PLD. At low substrate temperatures of 200 and 250 °C, the GaN thin films demonstrate poor crystallinity, a high defect density, and a rough surface morphology, resulting in FE-SEM images with low resolution and contrast. Conversely, at high substrate temperatures of 300, 350, and 400 °C, the GaN thin films exhibit improved crystallinity, a lower defect density, and a smoother surface morphology, leading to higher resolution and contrast in the FE-SEM images. The fabricated GaN/PSi nanostructures have a thickness of 2.426 μm.

Table 7 displays the thickness of the created GaN on PSi nanostructures at various temperatures, and it can be shown that the nanostructure has a thickness of 2.426 μm when it is fabricated at 300 °C. The average crystallite size, calculated using the Sherrer Eq. (2), decreases with decreasing film thickness in GaN on PSi nanostructures fabricated via the PLD process at substrate temperatures ranging from 200 to 400 °C. This trend can be attributed to several factors. One explanation is the increased likelihood of defects during thin film formation, such as dislocations and stacking faults. Smaller crystallites can develop at these flaws, which serve as nucleation sites. Moreover, strain and stress inside the thin film can also affect the size of the crystallites. Larger crystallites may break up into smaller ones as strain and stress levels rise due to reduced film thickness as referred in Tables 3 and 7.

Capabilities in electricity. *PSi substrate's electrical characteristics.* The current–voltage, capacitance–voltage, $1/C^2$ and voltage characteristics of the photodetector are shown in Fig. 18a–c, respectively.

As shown in Fig. 18a, a depletion region between the PSi and c-silicon resulting in a rectifying characteristic^{82,83}. As the voltage is applied, the current flowing through the PSi substrate increases due to charge transfer. On the other hand, Fig. 18b demonstrates a decrease in capacitance as the bias voltage increases from 0 to 3 V. This finding can be attributed to the expanding depletion region that occurs with increasing bias voltage, subsequently leading to a decrease in capacitance^{84,85}. The relationship between $1/C^2$ and voltage on a PSi substrate after fabrication is seen in Fig. 18c. The built-in potential was determined by extrapolating the linear segment of the curve to a $1/C^2$ value of 0 points. The calculated value of the built-in potential was found to be 0.34 V.

Electrical properties of GaN/PSi nano-structures. Figure 19 illustrates the dark I–V characteristics of GaN/PSi nanostructures fabricated at different substrate temperatures. It is observed that increasing the substrate temperatures from 200 to 300 °C results in improved crystallinity, reduced defect density, and increased carrier mobility. This can be attributed to the higher substrate temperature promoting better surface diffusion and increased mobility of adatoms, leading to the formation of high-quality crystalline structures. Furthermore, higher substrate temperatures can enhance the stoichiometry of the deposited films and reduce impurity incorporation. However, above 300 °C, the material properties begin to degrade due to thermal damage^{86,87}.

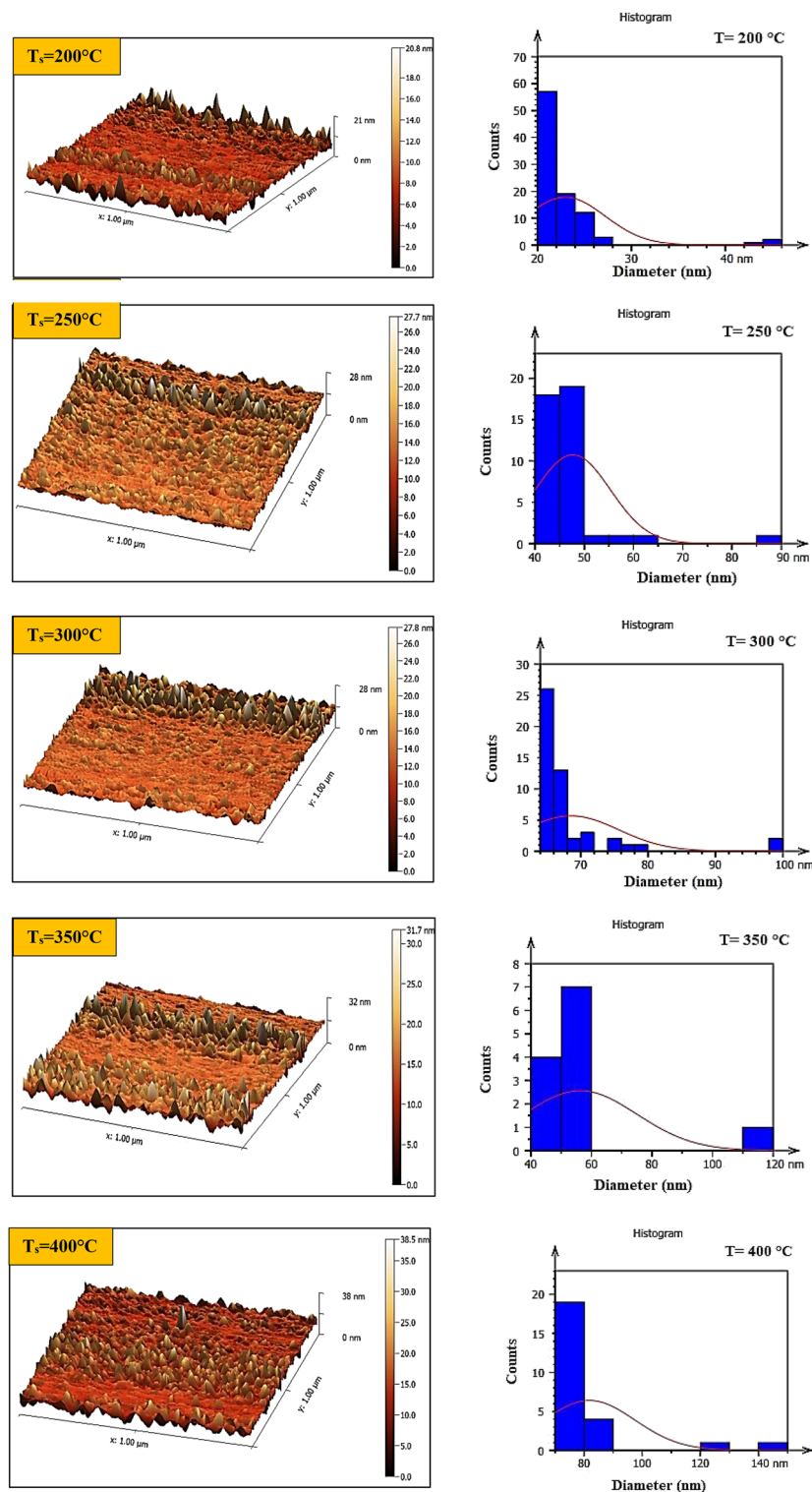


Figure 15. AFM and grain size distribution images of GaN/PSi nanostructures prepared at various substrate temperatures.

Figure 20 depicts the Capacitance vs voltage characteristics of GaN/PSi nanostructures fabricated using the PLD process at substrate temperatures ranging from 200 to 400 °C under an applied voltage of 0–2 V. The increase in capacitance observed at a substrate temperature of 300 °C can be attributed to an increase in the doping concentration and a decrease in the defect density. However, at temperatures above 300 °C, the capacitance decreases due to the formation of Ga clusters, which reduce the effective doping concentration^{40,88}.

T_s (°C)	Root-mean-square height (nm)	Average surface roughness (nm)	Average diameter (nm)
200	9.38	35.48	22.95
250	19.19	28.06	47.68
300	39.04	20.15	56.31
350	24.17	14.36	68.56
400	33.74	7.69	81.82

Table 6. AFM parameters of prepared GaN/Psi nanostructures using PLD process at different substrate temperatures 200 to 400 °C.

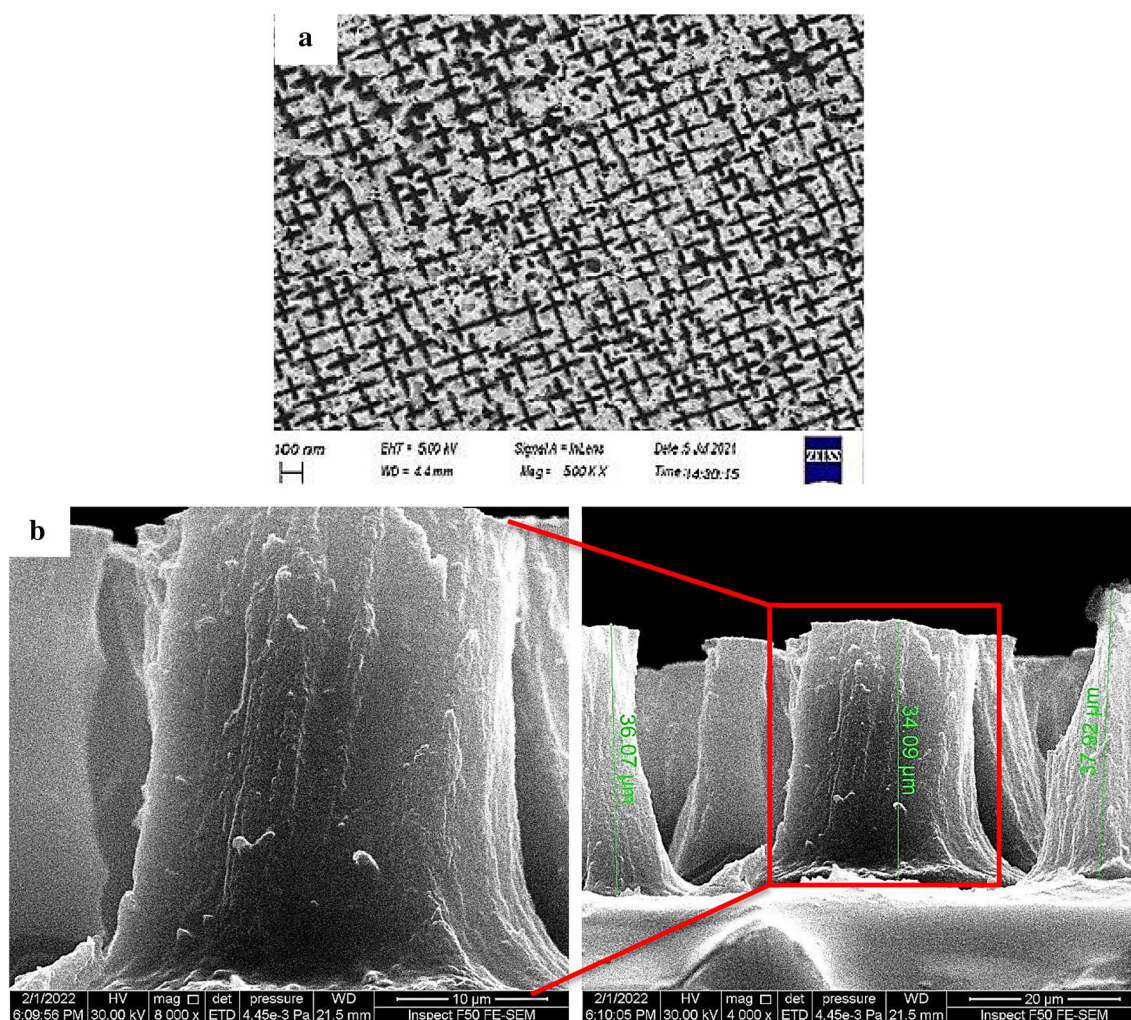


Figure 16. FE-SEM images of synthesized Psi substrate, (a) surface area image, and (b) cross -section image⁴⁴.

Figure 21 illustrates the $1/C^2$ versus voltage characteristics of GaN/Psi nanostructures fabricated using the PLD process on different substrates. The $1/C^2$ versus V characteristic is a plot of the inverse square of the capacitance, commonly used to analyze the interface properties of semiconductor devices. The built-in potential was found to be 0.32, 0.30, 0.21, 0.16, and 0.14 V at substrate temperatures of 200, 250, 300, 350, and 400 °C, respectively. It is observed that the built-in voltage of the GaN/Psi nanostructures decreases from 0.32 to 0.14 V, indicating a decrease in the defect density within the GaN/Psi nanostructure^{89,90}.

Effect of substrate temperatures on the performance properties of GaN/Psi heterojunction photodiode. The performance properties, including responsivity (R_λ), specific detectivity (D_λ), and external quantum efficiency (EQE), of the fabricated GaN/Psi heterojunction using the PLD method with optimal laser parameters (900 mJ laser energy, 355 nm laser wavelength) at different substrate temperatures, were determined

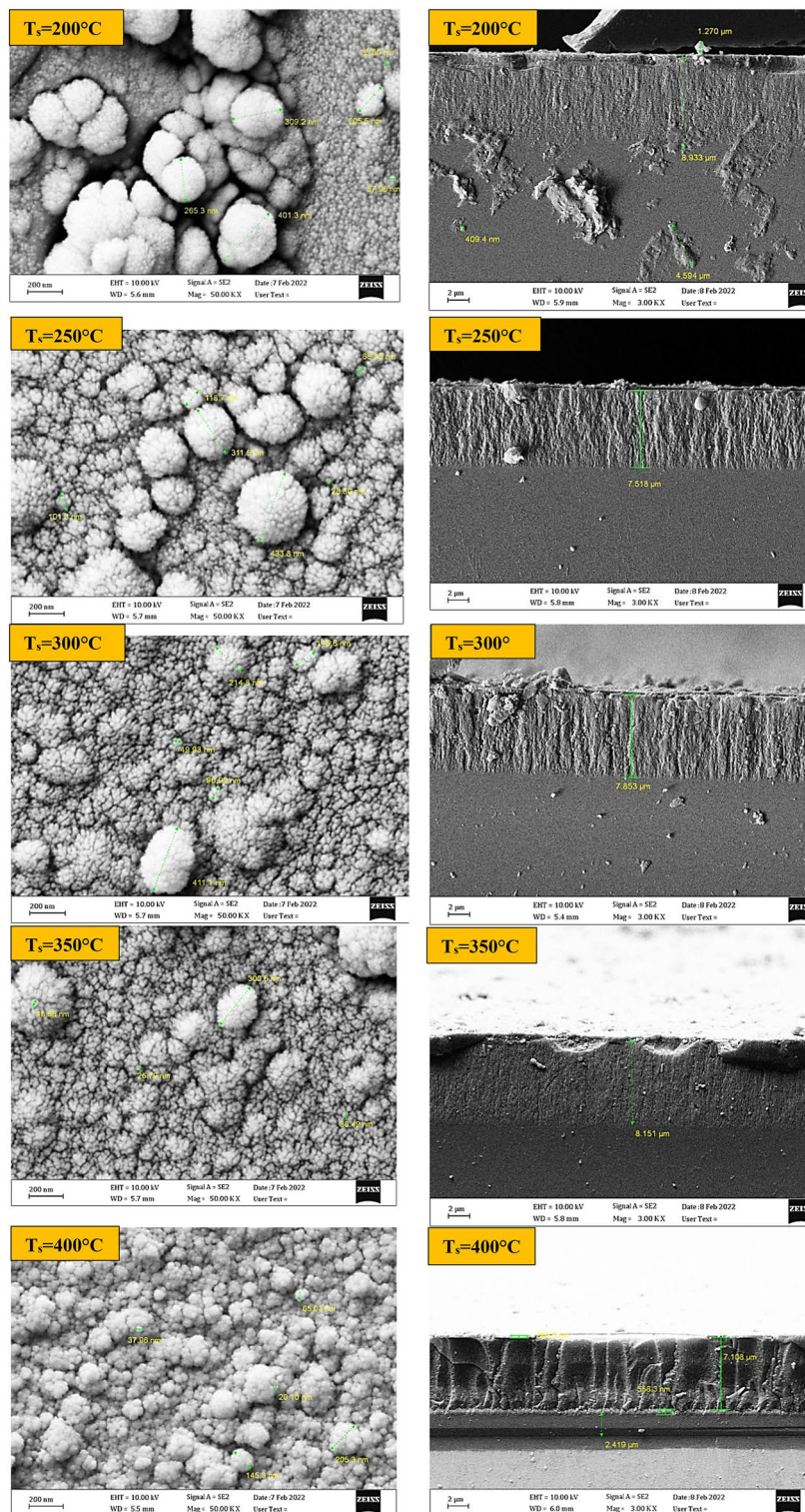


Figure 17. FE-SEM and cross-section images of GaN/PSi nanostructures made by the PLD process at substrate temperatures between 200 and 400 °C.

and are depicted in Figs. 22, 23, and 24. The equations representing R_{λ} , D_{λ} , and EQE are given as Eqs. (6), (7), and (8), respectively^{91,92}.

$$R_{\lambda} = \frac{I_{ph}}{P} \tag{7}$$

Substrate temperature (°C)	Thickness (μm)
200	3.8
250	3.5
300	2.42
350	2.3
400	2.2

Table 7. The thickness of GaN films deposited on P-Si substrate at laser energy of 900 mJ as a function of substrate temperature.

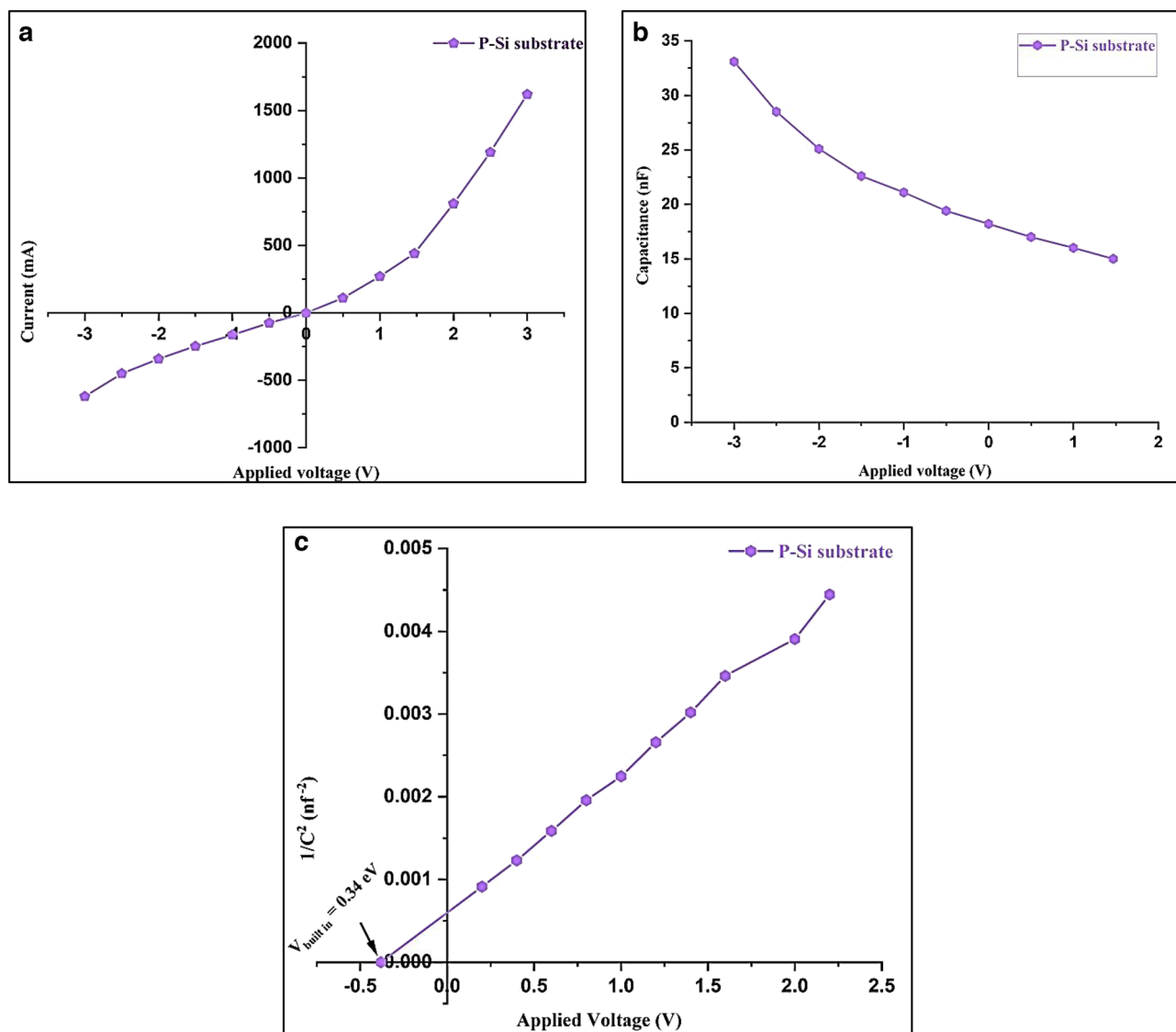


Figure 18. (a) Dark I–V characteristics at forward and reverse, (b) C–V characteristics, and (c) $1/C^2$ versus voltage^{42,43}.

where I_{ph} is the photocurrent (Ampere), and P is the incident power (Watt). The specific detectivity D^* is given by^{93,94}:

$$(D^*_\lambda) = \frac{R_\lambda \sqrt{A}}{\sqrt{2qI_d}} \tag{8}$$

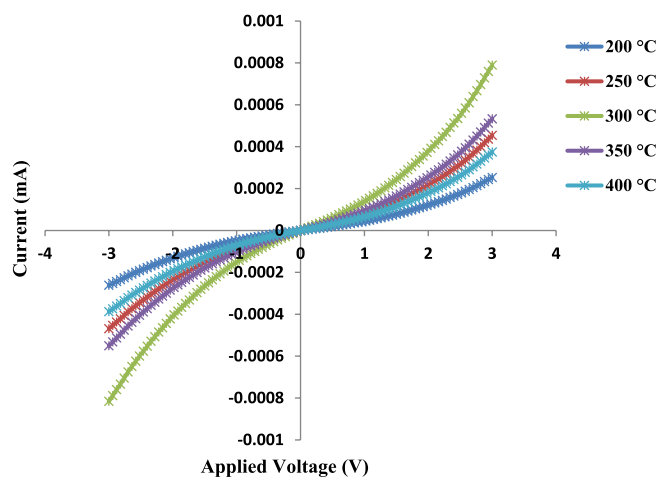


Figure 19. PLD-fabricated GaN/PSi nanostructure dark I–V properties at substrate temperatures between 200 and 400 °C under forward and reverse biases.

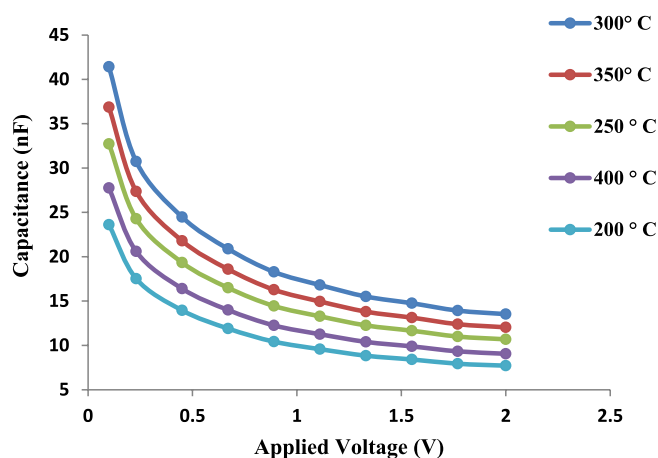


Figure 20. C–V characteristics of GaN/PSi nanostructures made by the PLD process at substrate temperatures between 200 and 400 °C.

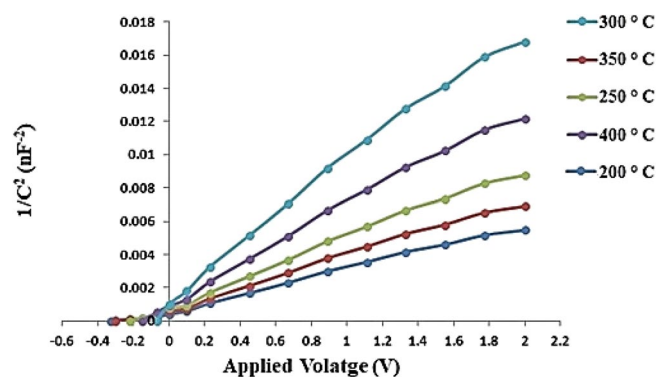


Figure 21. $1/C^2$ –V characteristics of GaN/PSi nanostructures made by the PLD process at substrate temperatures between 200 and 400 °C.

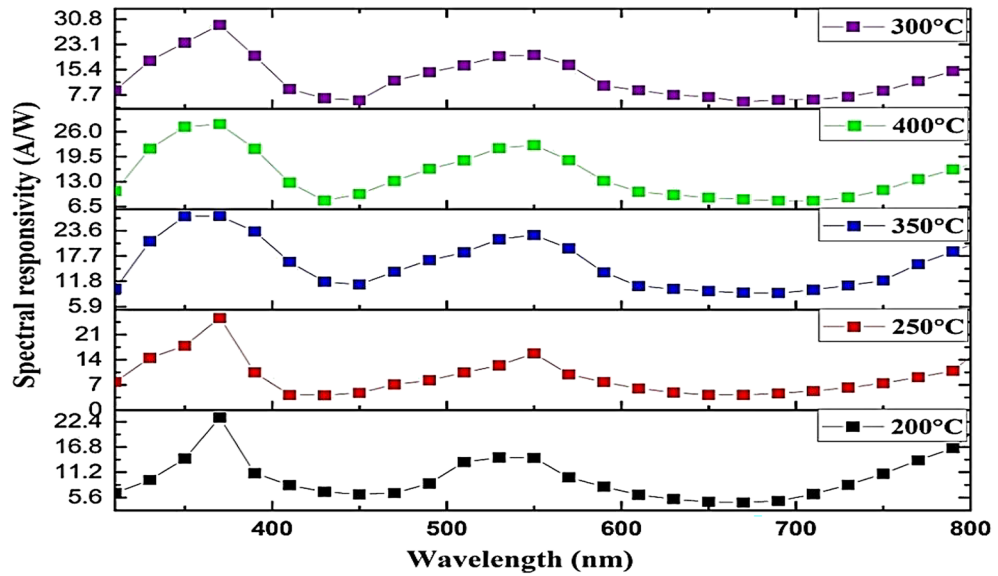


Figure 22. Spectral responsivity of GaN/PSi heterojunction photodetectors fabricated at various substrate temperatures.

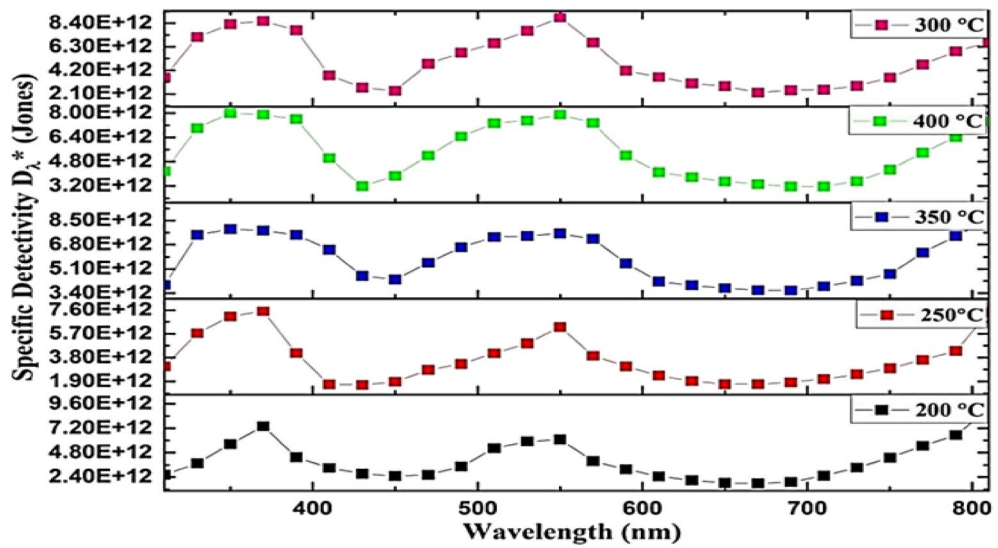


Figure 23. Specific detectivity of GaN/PSi nanostructures made by the PLD process at substrate temperatures between 200 and 400 °C.

where A is the area of photodetector, I_d is the dark current of photodetector, and q is the electron charge. The eternal quantum efficiency can be given by^{95,96}:

$$(EQE) = \frac{1240 R_\lambda}{\lambda_{nm}} \tag{9}$$

The wavelength of the incident photon is denoted by λ , while the spectral responsivity is denoted by R_λ .

Figure 22 illustrates the measured spectral responsivity of fabricated GaN/PSi heterojunction photodiode using the PLD process at different substrate temperatures from 200 to 400 °C. It's observed that the responsivity increased with increasing substrate temperature up to 300 °C and then decreased at higher temperatures of 350 and 400 °C. They attributed this behaviour to increased crystalline quality and reduced defect density of the fabricated GaN/PSi nano-structures photodiode at higher substrate temperatures (350 and 400 °C)^{97,98}. The high responsivity of the fabricated photodetectors is due to the presence of two heterojunctions: GaN/PSi and PSi/C-Si. Two response peaks are found at 380 and 540 nm, with the first one being attributed to the absorption

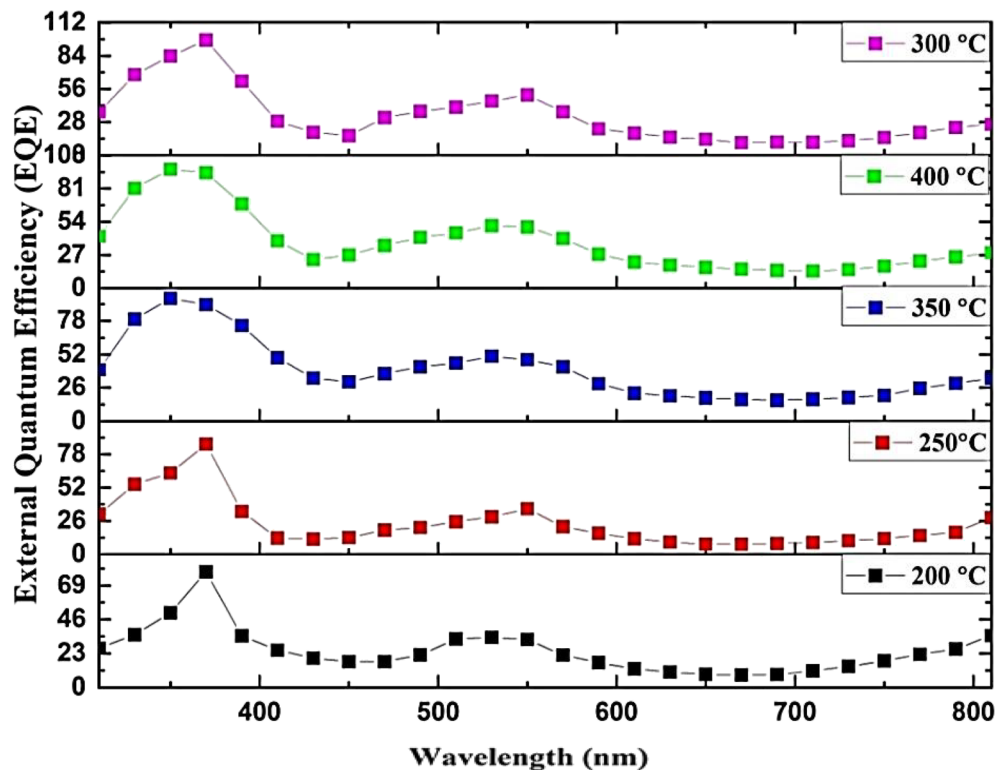


Figure 24. Impact of substrate temperature on the EQE of the photodetectors.

edge of the GaN film, while the second peak belongs to the porous silicon substrate. The maximum responsivity was 29.03 A/W at 380 nm and 19.86 A/W at 540 nm for the photodetector prepared at a substrate temperature of 300 °C. We believe that the reason behind this finding is the large depletion width that extends toward the film surface, enhancing the responsivity of short wavelengths. When the film thickness is reduced, it results in an increased transmission of photons to the silicon substrate, especially for those with wavelengths (λ) greater than the GaN cut-off wavelength ($\lambda_{\text{cut-off}}$). This phenomenon leads to photon absorption in the porous silicon substrate, thereby enhancing responsivity in the visible region^{99,100}.

In addition, Fig. 23 illustrates the specific detectivity of the fabricated GaN/PSi nanostructures. It is observed that the density of defects decreases as the substrate temperature increases. Consequently, a substrate temperature of 300 °C is determined to be the optimal condition during the PLD growth process to achieve high-quality GaN/PSi nanostructures.

The computed EQE of a PLD-process-fabricated GaN/PSi heterojunction photodiode at substrate temperatures ranging from 200 to 400 °C is shown in Fig. 24. It's observed the EQE increased with increasing substrate temperature from 200 to 300 °C, and then decreased at higher temperatures of 350 and 400 °C. They attributed this behaviour to improving crystal quality at higher substrate temperatures, which reduced the non-radiative recombination centres and enhanced the radiative recombination^{101,102}.

All of the GaN/PSi heterojunction photodetectors listed in Table 8 were measured at 100 mW/cm² using a Keithley 2400, and their switching characteristics are presented in Figs. 25 and 26 for substrate temperatures ranging from 200 to 400 °C. The switching tests consisted of three separate cycles, each lasting 25 s on and 18 s off. The rise time of the photodiodes was measured from 10 to 90% of the peak signal, while the fall time was measured from 90 to 10% of the peak signal, as depicted in Fig. 26. It is observed that increasing the substrate temperature from 200 to 300 °C during the PLD growth process of GaN thin films results in a reduction in the rise time and fall time of electronic devices based on GaN, owing to the improvement in crystalline quality. Specifically, at 300 °C, the fabricated GaN/PSi nanostructure photodiode exhibited a rise time of 328 μ s and a fall time of 617 μ s.

The GaN/PSi heterojunction photodiodes fabricated using the PLD process at different substrate temperatures exhibit superior performance characteristics in the UV-A band (370 nm) and yellow band (575 nm). The spectral responsivity of the photodiodes is measured to be 29.03 A/W and 19.86 A/W, with detectivity values of 8.6×10^{12} and 8.9×10^{12} Jones, and external quantum efficiency values of 97.2% and 50.89%, respectively. These photodiodes also demonstrate fast response times, with a rise time of 363 μ sec and a fall time of 711 μ s. These performance metrics surpass those achieved by Jiang et al. (2022), who fabricated a GaN/Si UV photodetector

T_s (°C)	R_i (A/W)	$D^*_{\lambda} \times 10^{12}$ (Jones)	EQE (%)	τ_r (μ s)	τ_f (μ s)
200	23.36 at 370 nm	7.4	78.28	355	702
	14.46 at 550 nm	6.1	33.8		
250	25.62 at 370 nm	7.5	85.88	374	679
	15.78 at 555 nm	6.2	35.5		
300	29.03 at 370 nm	8.6	97.2	363	711
	19.86 at 575 nm	8.9	50.89		
350	27.05 at 370 nm	7.8	90.6	327	652
	22.57 at 555 nm	7.6	47.9		
400	28.02 at 370 nm	7.9	93.9	370	702
	22.05 at 555 nm	7.9	49.7		

Table 8. Figures of merit of GaN/PSi nanostructures photodetector fabricated at various substrate temperatures.

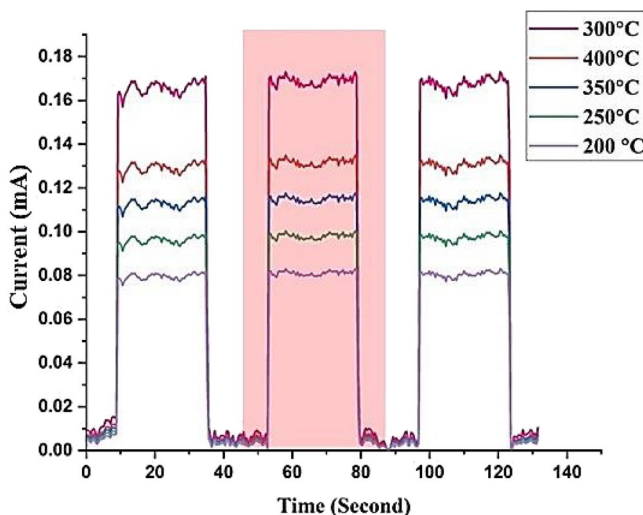


Figure 25. A switching characteristic of fabricated GaN/PSi heterojunction photodiode at different substrate temperatures.

using a chemical vapor deposition process, which had a responsivity of 71.4 mA/W, detectivity of 7.1×10^8 Jones, external quantum efficiency of 24.3%, and response time of 0.2/7.6 s^{103,104}.

Conclusion

The GaN/PSi nanostructures were successfully fabricated as heterojunction photodiodes using the pulsed laser deposition method with a 300 nm laser wavelength, 900 mJ laser energy, and different substrate temperatures ranging from 200 to 400 °C. All of the GaN/PSi heterojunction photodiodes exhibited prominent crystalline peaks with large crystallite sizes at 300 °C. Photoluminescence measurements revealed peaks at 368 nm and 728 nm, corresponding to energy gaps of 3.36 eV and 1.7 eV, respectively, which are in agreement with the theoretical values for GaN and PSi energy gaps. The morphological structure of the nanostructures exhibited a cauliflower-like shape, while the topography properties displayed a roughness of 20.15 nm and an average diameter of 56.31 nm. The spectral responsivity analysis demonstrated that all of the heterojunction photodiodes functioned effectively in UV-A and Green band photodetection. The responsivity generally increased with increasing substrate temperature up to 300 °C, beyond which it decreased due to the degradation in the crystalline quality of the GaN thin films. Consequently, a significantly improved UV photodetection capability was achieved through this novel laser technique. The optimal substrate temperature for maximizing the responsivity was found to be 300 °C, resulting in responsivity values of 23.36 at 370 nm and 14.46 at 550 nm. The detectivity values were measured to be 8.6×10^{12} and 8.9×10^{12} Jones, with external quantum efficiencies of 97.2% and 50.89%, respectively. The substrate temperature of 300 °C during the fabrication of GaN/PSi nanostructures had a significant impact on their electrical properties. While higher substrate temperatures (350 and 400 °C) can lead to improved crystallinity, reduced defect density, and increased carrier mobility, temperatures above 300 °C can cause degradation in the material properties due to thermal damage.

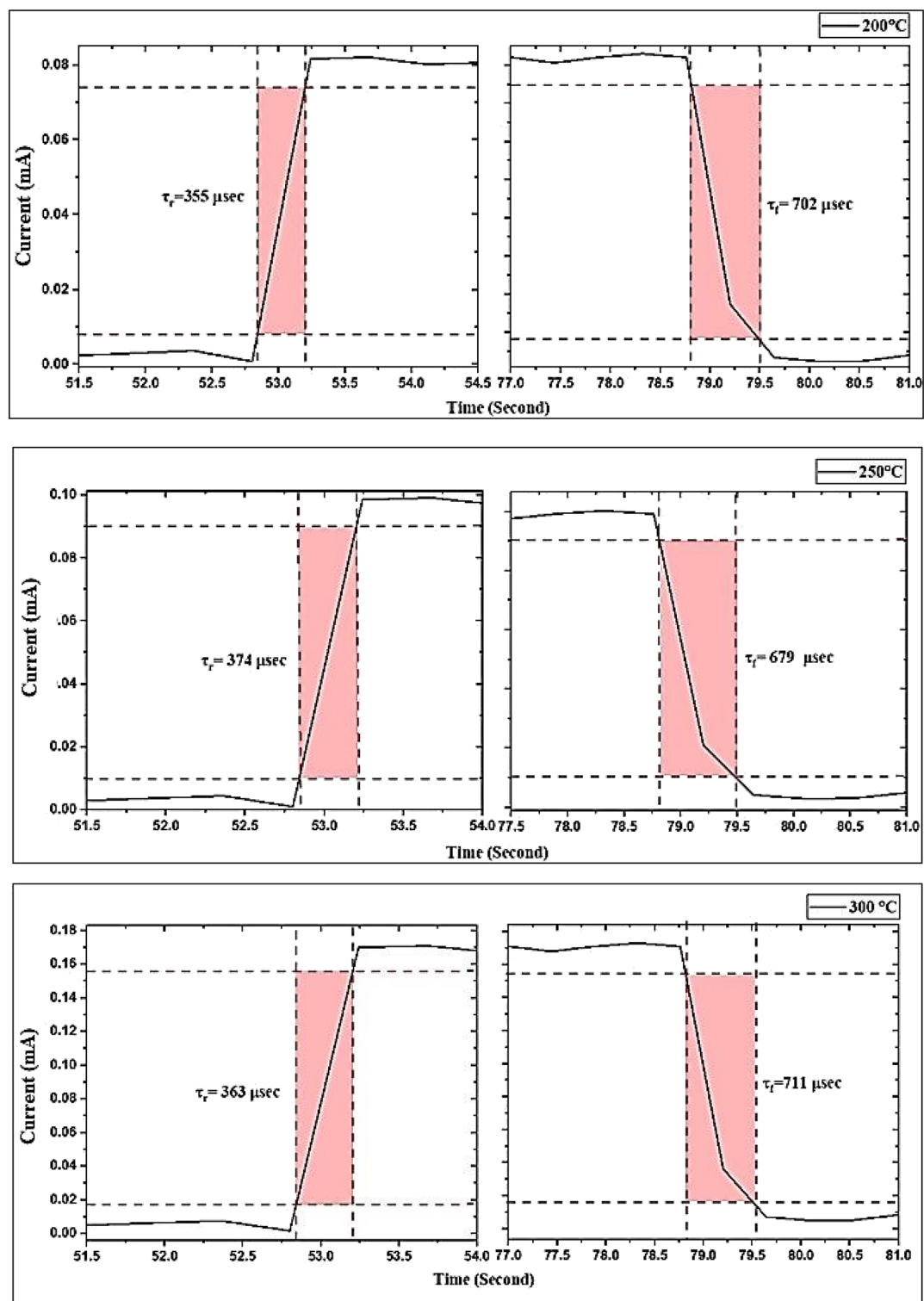


Figure 26. Rise time and fall time of GaN/PSi nanostructures made by the PLD process at substrate temperatures between 200 and 400 °C.

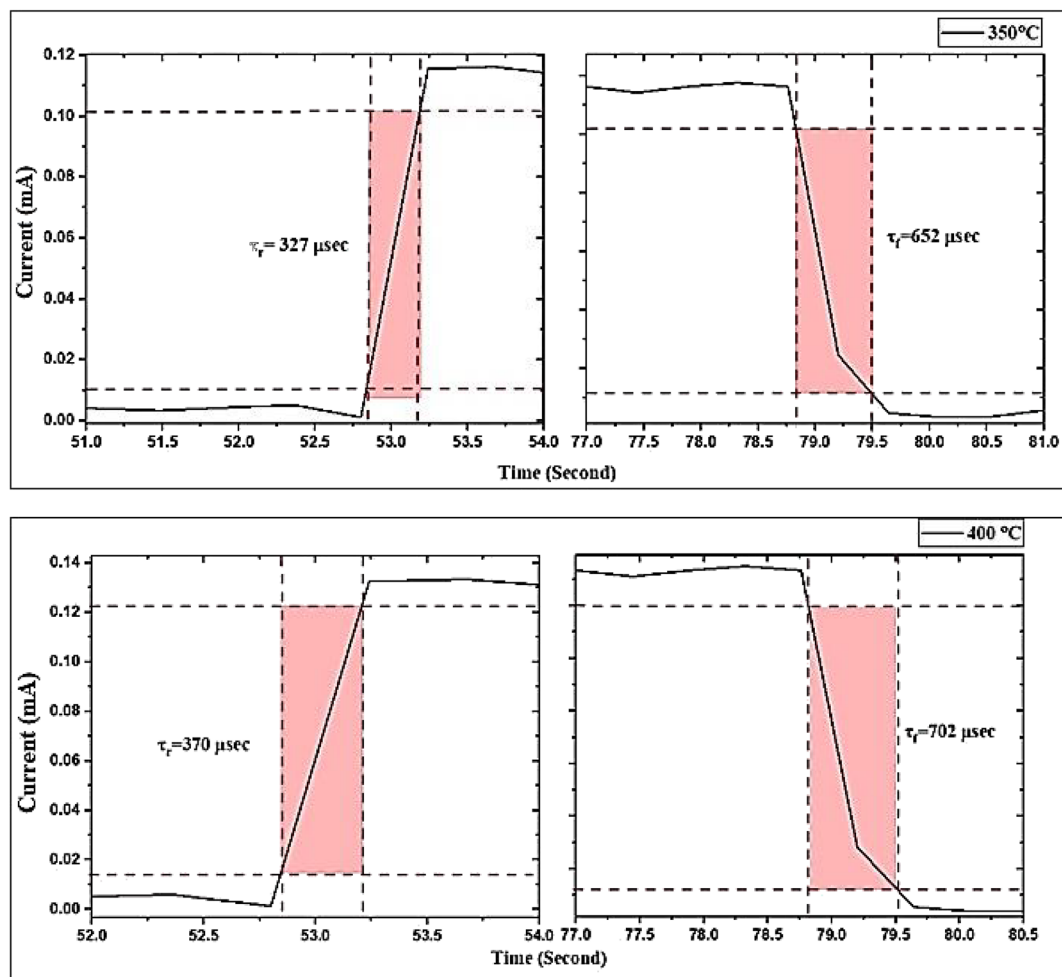


Figure 26. (continued)

Data availability

Correspondence and requests for materials should be addressed to Makram A. Fakhri, Haneen D. Jabbar, and Evan T. Salim.

Received: 13 April 2023; Accepted: 25 August 2023

Published online: 07 September 2023

References

1. Edmond, J. *et al.* High efficiency GaN-based LEDs and lasers on SiC. *J. Cryst. Growth* **272**(1–4), 242–250 (2004).
2. Amir, H. A. A. *et al.* Synthesis of gallium nitride nanostructure using pulsed laser ablation in liquid for photoelectric detector. *Mater. Sci. Semicond. Process.* **150**, 106911 (2022).
3. Rigutti, L. *et al.* Ultraviolet photodetector based on GaN/AlN quantum disks in a single nanowire. *Nano Lett.* **10**(8), 2939–2943 (2010).
4. Fakhri, M. A. *et al.* Synthesis and characterization of GaN/quartz nanostructure using pulsed laser ablation in liquid. *Phys. Scr.* **97**, 115813. <https://doi.org/10.1088/1402-4896/ac9866> (2022).
5. Jiang, J. *et al.* Improved ultraviolet emission performance from polarization-engineered n-ZnO/p-GaN heterojunction diode. *Appl. Phys. Lett.* **108**(6), 063505 (2016).
6. Amir, H. A. A. *et al.* An investigation on GaN/Porous-Si NO₂ gas sensor fabricated by pulsed laser ablation in liquid. *Sens. Actuators B Chem.* **367**, 132163 (2022).
7. Adivarahan, V. *et al.* 280 nm deep ultraviolet light emitting diode lamp with an AlGaIn multiple quantum well active region. *Appl. Phys. Express* **2**(10), 102101 (2009).
8. Abdul Amir, H. A. A., Fakhri, M. A. & Alwahib, A. A. Review of GaN optical device characteristics, applications, and optical analysis technology. *Mater. Today Proc.* **42**, 2815–2821 (2021).
9. Khan, M. A., Bhattarai, A., Kuznia, J. N. & Olson, D. T. High electron mobility transistor based on a GaN-AlxGa1-xN heterojunction. *Appl. Phys. Lett.* **63**, 1214 (1993).
10. Abdul Amir, H. A. A., Fakhri, M. A., Alwahib, A. A. & Salim, E. T. Optical investigations of GaN deposited nano films using pulsed laser ablation in ethanol. *Int. J. Nanoelectron. Mater.* **15**(2), 129–138 (2022).
11. Wu, Y.-F. GaN-based FET's for microwave power amplification. *IEICE Trans. Electron.* **82**(11), 1895 (1999).
12. Jabbar, H. D., Fakhri, M. A. & AbdulRazzaq, M. J. Gallium nitride-based photodiode: A review. *Mater. Today Proc.* **42**, 2829–2834 (2021).

13. Chen, Q. High transconductance AlGa_N/Ga_N heterostructure field effect transistors on SiC substrates. *Electron. Lett.* **33**, 1413 (1997).
14. Sheppard, S. T. High-power microwave Ga_N/AlGa_N HEMT on semi-insulating silicon carbide substrates. *IEEE Electron Device Lett.* **20**, 161 (1999).
15. Salim, E. T. Surface morphology and X-ray diffraction analysis for silicon nanocrystal-based heterostructures. *Surf. Rev. Lett.* **20**(05), 1350046 (2013).
16. Wong, K. Y., Chen, W., Liu, X., Zhou, C. & Chen, K. J. Ga_N smart power IC technology. *Phys. Status Solidi (b)* **247**(7), 1732–1734 (2010).
17. Ji, H. *et al.* Yellow electroluminescence realized in Ga_N/Si nanoheterostructures based on silicon nanoporous pillar array. *J. Lumin.* **199**(194–199), 10 (2018).
18. Ismail, R. A., Habubi, N. F. & Abbod, M. M. Preparation of high-sensitivity In₂S₃/Si heterojunction photodetector by chemical spray pyrolysis. *Opt. Quant. Electron.* **48**, 455 (2016).
19. Würtele, M. A. *et al.* Application of Ga_N-based ultraviolet-C light emitting diodes–UV LEDs–for water disinfection. *Water Res.* **45**(3), 1481–1489 (2011).
20. Ohno, Y. & Kuzuhara, M. Application of Ga_N-based heterojunction FETs for advanced wireless communication. *IEEE Trans. Electron Devices* **48**(3), 517–523 (2001).
21. Abdulrazzaq, O. A. & Saleem, E. T. Inexpensive near-IR photodetector. *Turk. J. Phys.* **30**, 35–39 (2006).
22. Sun, R., Lai, J., Chen, W. & Zhang, B. Ga_N power integration for high frequency and high efficiency power applications: A review. *IEEE Access* **8**(15529–15542), 13 (2020).
23. Zhang, X. *et al.* Design and integration of a layered MoS₂/Ga_N van der Waals heterostructure for wide spectral detection and enhanced photoresponse. *ACS Appl. Mater. Interfaces* **12**(42), 47721–47728 (2020).
24. Ismail, R. A. Fabrication and characterization of photodetector based on porous silicon. *e-J. Surf. Sci.* **8**, 388–391 (2010).
25. Cai, Y. *et al.* Nonpolar (11 $\bar{2}$ 0) Ga_N metal–semiconductor–metal photodetectors with superior performance on silicon. *ACS Appl. Mater. Interfaces* **12**(22), 25031–25036 (2020).
26. Wasisto, H. S., Prades, J. D., Güllink, J. & Waag, A. Beyond solid-state lighting: Miniaturization, hybrid integration, and applications of Ga_N nano- and micro-LEDs. *Appl. Phys. Rev.* **6**(4), 041315 (2019).
27. Ismail, R. A., Yehya, K. Z. & Abdulrazzaq, O. A. Preparation and photovoltaic properties of Ag₂O/Si isotype heterojunction. *Surf. Rev. Lett.* **12**, 299–303 (2005).
28. Sood, A. K., Zeller, J. W., Ghuman, P., Babu, S., Dupuis, R. D. High performance Ga_N/AlGa_N ultraviolet avalanche photodiode detector technologies. Proc. SPIE 10980, Image Sensing Technologies: Materials, Devices, Systems, and Applications VI, 109800M (2019) <https://doi.org/10.1117/12.2521464>.
29. Zhang, Y., Li, J. & Wang, J. Investigations on driver and layout for paralleled Ga_N HEMTs in low voltage application. *IEEE Access* **7**(179134–179142), 18 (2019).
30. Salim, E. T. Rapid thermal oxidation for silicon nanocrystal based solar cell. *Int. J. Nanoelectron. Mater.* **5**(2), 95–100 (2012).
31. Liu, B., Boon, C. C., Mao, M., Choi, P. & Guo, T. A 2.4–6 GHz broadband Ga_N power amplifier for 802.11 ax application. *IEEE Trans. Circuits Syst. I Regular Pap.* **68**(6), 2404–2417 (2021).
32. Shu, H., Niu, X., Ding, X. & Wang, Y. Effects of strain and surface modification on stability, electronic and optical properties of Ga_N monolayer. *Appl. Surf. Sci.* **479**, 475–481 (2019).
33. Fakhri, M. A. *et al.* Fabrication of UV photodetector based on Ga_N/Psi heterojunction using pulse laser deposition method: Effect of different laser wavelengths. *Opt. Mater.* **137**, 113593 (2023).
34. Farah, Z. J., Mohammed, J. A.-R. & Hisham, M. A. Design of Ga_N-based VCSEL with high performance. *Otoelectronics Adv. Mater. Rapid Commun.* **8**(1–2), 7–9 (2014).
35. Barbosa, M. B., Correia, J. G., Lorenz, K., Vianden, R. & Araújo, J. P. Studying electronic properties in Ga_N without electrical contacts using γ - γ vs e - γ perturbed angular correlations. *Sci. Rep.* **9**(1), 1–13 (2019).
36. Muhsien, M. A., Salim, E. T., Al-Douri, Y., Sale, A. F. & Agool, I. R. Synthesis of SnO₂ nanostructures employing Nd:YAG laser. *Appl. Phys. A* **120**(2), 725–730 (2015).
37. Eason, R. (ed.) *Pulsed Laser Deposition of Thin Films: Applications-Led Growth of Functional Materials* (Wiley, 2007).
38. Baig, M. K. *et al.* Pulsed laser deposition of SmCo thin films for MEMS applications. *J. Appl. Res. Technol.* **14**(5), 287–292 (2016).
39. Salim, E. T., Fakhri, M. A. & Hassen, H. Metal oxide nanoparticles suspension for optoelectronic devices fabrication. *Int. J. Nanoelectron. Mater.* **6**(2), 121–128 (2013).
40. Gad, S., Fathy, M., Badr, Y. & Kashyout, A. E. H. B. Pulsed laser deposition of In_{0.1}Ga_{0.9}N nanoshapes by Nd: YAG technique. *Coatings* **10**(5), 465 (2020).
41. Guo, C. & Singh, S. C. (eds) *Handbook of Laser Technology and Applications: Lasers Applications: Materials Processing and Spectroscopy* Vol. 3 (CRC Press, 2021).
42. Jabbar, H. D., Fakhri, M. A. & AbdulRazzaq, M. J. Synthesis gallium nitride on porous silicon nano-structure for optoelectronics devices. *SILICON* **14**, 12837–12853 (2022).
43. Ougua, S. N., Ntwaeaborwa, O. M. & Swart, H. C. Latest development on pulsed laser deposited thin films for advanced luminescence applications. *Coatings* **10**(11), 1078 (2020).
44. Jabbar, H. D. *et al.* Effect of different etching time on fabrication of an optoelectronic device based on Ga_N/Psi. *J. Renew. Mater.* **11**(3), 1101–1122 (2023).
45. Aziz, M. J. Film growth mechanisms in pulsed laser deposition. *Appl. Phys. A* **93**, 579–587 (2008).
46. Craciun, F., Lippert, T. & Dinescu, M. Pulsed laser deposition: Fundamentals, applications, and perspectives. In *Handbook of Laser Micro- and Nano-engineering* 1291–1323 (Springer, 2021).
47. Manoj, K. C. M. *et al.* Optimized aluminum reflector for enhancement of UVC cathodoluminescence based-AlGa_N materials with carbon nanotube field emitters. *Molecules* **26**(13), 4025 (2021).
48. Wael, Z. T. *et al.* Cathodoluminescence of a 2 inch ultraviolet-light-source tube based on the integration of AlGa_N materials and carbon nanotube field emitters. *J. Mater. Chem. C* **7**, 11540–11548 (2019).
49. Jabar, H. D., Fakhri, M. A., AbdulRazzaq, M. J. & Gopinath, S. C. The structural and optical investigation of grown Ga_N film on porous silicon substrate prepared by PLD. *Eng. Technol. J.* **41**(2), 270–279 (2023).
50. Ahmed, N. *Biomedical Science Practice: Experimental & Professional Skills* (Oxford University Press, 2016).
51. Omar, K. & Salman, K. A. Effects of electrochemical etching time on the performance of porous silicon solar cells on crystalline n-type (100) and (111). *J. Nano Res.* **46**, 45–56 (2017).
52. Salim, E. T., Al-Wazny, M. S. & Fakhri, M. A. Glancing angle reactive pulsed laser deposition (GRPLD) for Bi₂O₃/Si heterostructure. *Mod. Phys. Lett. B* **27**(16), 1350122. <https://doi.org/10.1142/S0217984913501224> (2013).
53. Kang, B. K. *et al.* Formation of highly efficient dye-sensitized solar cells by effective electron injection with Ga_N nanoparticles. *J. Electrochem. Soc.* **158**(7), H693 (2011).
54. Al-Douri, Y. *et al.* Structural properties and surface morphology analysis of nanophotonic LINBO₃. *ARPN J. Eng. Appl. Sci.* **11**(8), 4974–4978 (2016).
55. Wahid, M. H. A., Abdulwahhab, A. W., Salim, Z. T. & Hashim, U. Heat treatment assisted-spin coating for LiNbO₃ films preparation: Their physical properties. *J. Phys. Chem. Solids* **131**, 180–188. <https://doi.org/10.1016/j.jpics.2019.03.033> (2019).

56. Abood, M. K., Halim, M., Wahid, A., Salim, E. T. & Admon, J. Niobium pentoxide thin films employ simple colloidal suspension at low preparation temperature. *Eur. Phys. J. Conf.* **162**(12), 01058 (2017).
57. Koch, C. C., Ovid'Ko, I. A., Seal, S. & Veprek, S. *Structural Nanocrystalline Materials: Fundamentals and Applications* (Cambridge University Press, 2007).
58. Ismail, R. A., Khashan, K. S. & Alwan, A. M. Study of the effect of incorporation of CdS nanoparticles on the porous silicon photodetector. *SILICON* **9**, 321–326 (2017).
59. Salim, E. T., Agoool, I. R. & Muhsien, M. A. Construction of SnO₂/SiO₂/Si heterojunction and its lineup using I-V and C-V measurements. *Int. J. Mod. Phys. B* **25**(29), 3863–3869 (2011).
60. Swanson, W. E. *Tables for Conversion of X-ray Diffraction Angles to In-terplanar Spacing* (National Bureau of Standards, 1960).
61. Fakhri, M. A. *et al.* Responsivity and response time of nano silver oxide on silicon heterojunction detector. *Int. J. Nanoelectr. Mater.* **11**(Special Issue BOND21), 65–72 (2018).
62. Pushkarev, S. S., Grekhov, M. M. & Zenchenko, N. V. X-ray diffraction analysis of features of the crystal structure of GaN/Al 0.32 Ga 0.68 N HEMT-heterostructures by the Williamson-Hall method. *Semiconductors* **52**, 734–738 (2018).
63. Wang, T. *et al.* Structure and photoluminescence properties of the quasi-regular arrangements of porous silicon. *Optoelectronics Adv. Mater.-Rapid Commun.* **5**(2011), 495–498 (2011).
64. Hassanien, A. S. & Akl, A. A. Effect of Se addition on optical and electrical properties of chalcogenide CdSse thin films. *Superlattices Microstruct.* **89**, 153–169 (2016).
65. Al-Douri, Y., Fakhri, M. A., Badi, N. & Voon, C. H. Effect of stirring time on the structural parameters of nanophotonic LiNbO₃ deposited by spin-coating technique. *Optik* **156**, 886–890 (2018).
66. Canham, C. D. Suppression and release during canopy recruitment in *Fagus grandifolia*. *Bull. Torrey Bot. Club* **1–7** (1990).
67. Abdulwahhab, A. W., Hashim, U., Minshid, M. A. & Salim, Z. T. The effect of annealing temperature on optical and photolumence properties of LiNbO₃. *Surf. Rev. Lett.* **26**(10), 1950068. <https://doi.org/10.1142/S0218625X19500689> (2019).
68. Jabbar, H. D., AbdulRazzaq, M. J. & Fakhri, M. A. Synthesis porous silicon substrates using electrochemical etching method assisted by laser. *AIP Conf. Proc.* **2660**, 020126. <https://doi.org/10.1063/5.0107762> (2022).
69. Fakhri, M. A. *et al.* Synthesis of nano porous silicon heterostructures for optoelectronic applications. *AIP Conf. Proc.* **2045**, 020016. <https://doi.org/10.1063/1.5080829> (2018).
70. Shi, J., Yu, L., Wang, Y., Zhang, G. & Zhang, H. Influence of different types of threading dislocations on the carrier mobility and photoluminescence in epitaxial GaN. *Appl. Phys. Lett.* **80**(13), 2293–2295 (2002).
71. Asady, H., Salim, E. T. & Ismail, R. A. Some critical issues on the structural properties of Nb₂O₅ nanostructure film deposited by hydrothermal technique. *AIP Conf. Proc.* **2213**(1), 020183 (2020).
72. Martínez-Ara, L. A., Aguilar-Hernández, J. R., Sastré-Hernández, J., Hernández-Hernández, L. A., Hernández-Pérez, M. d. l. A., Maldonado-Altamirano, P., Mendoza-Pérez, R., & Contreras-Puente, G. Structural and optical properties of GaN thin films grown on Si (111) by pulsed laser deposition. *Mater. Res.* **22**(2), e20180263. <https://doi.org/10.1590/1980-5373-MR-2018-0263> (2019).
73. Zambrano-Serrano, M. A. *et al.* Effects of heavy Si doping on the structural and optical properties of n-GaN/AlN/Si (111) heterostructures. *Mater. Res. Express* **9**(6), 065903 (2022).
74. Myrick, M. L. *et al.* The Kubelka-Munk diffuse reflectance formula revisited. *Appl. Spectrosc. Rev.* **46**(2), 140–165 (2011).
75. Ismail, R. A., Rasheed, B. G., Salm, E. T. & Al-Hadethy, M. High transmittance-low resistivity cadmium oxide films grown by reactive pulsed laser deposition. *J. Mater. Sci. Mater. Electron.* **18**(10), 1027–1030 (2007).
76. AbdulRazzaq, M. J., Shibib, K. S. & Younis, S. I. Temperature distribution and stress analysis of end pumped lasers under Gaussian pump profile. *Opt. Quantum Electron.* **52**, 379 (2020).
77. Wahid, M. H. A., Abdulwahhab, A. W., Hashim, U. & Salim, Z. T. Efficiency enhancement of optical strip waveguide by the effect of heat treatment. *Optik* **180**, 768–774. <https://doi.org/10.1016/j.jjleo.2018.12.006> (2019).
78. Yadav, G., Jindal, K. & Tomar, M. Influence of pulsed laser deposited hafnium oxide thin film as gate dielectric on the fabrication of Al_{0.1}Ga_{0.9}N/GaN MOS-HEMT. *Mater. Sci. Semicond. Process.* **153**, 107136 (2023).
79. Zheng, X. X., Lin, C. H., Ueda, D. & Chang, E. Y. Effects of the growth temperature on structural and electrical properties of AlN/GaN heterostructures grown by metal organic chemical vapor deposition. *Thin Solid Films* **709**, 138228 (2020).
80. Salim, E. T. Optoelectronic properties of Fe₂O₃/Si heterojunction prepared by rapid thermal oxidation method. *Indian J. Phys.* **87**(4), 349–353. <https://doi.org/10.1007/s12648-012-0229-5> (2013).
81. Muhammed, Q. Q., Saleh, M. M., Al-Azawi, R. J., Kadhim, A. C., & Shaker, R. M., Close-range photogrammetric techniques for investigating and documenting the ancient buildings, in *Optics InfoBase Conference Papers*, JTU5A.91 (2022).
82. Pujadó, M. P. *Carbon Nanotubes as Platforms for Biosensors with Electrochemical and Electronic Transduction* (Springer, 2012).
83. Agoool, I. R. & SalimHassan, E. T. M. A. Muhsien, optical and electrical properties of SnO₂ thin film prepared using RTO method. *Int. J. Mod. Phys. B* **25**(8), 1081–1089. <https://doi.org/10.1142/S0217979211058614> (2011).
84. Abd, A. N., Habubi, N. F., Reshak, A. H., & Mansour, H. L. (2018). Enhancing the electrical properties of porous silicon photodetector by depositing MWCNTs. *Int. J. Nanoelectr. Mater.* **11**(3).
85. Hassan, M. A. M., Al-Kadhemy, M. F. H. & Salem, E. T. Effect irradiation time of Gamma ray on MSISM (Au/SnO₂/SiO₂/Si/Al) devices using theoretical modeling. *Int. J. Nanoelectr. Mater.* **8**(2), 69–82 (2014).
86. Lee, M. *et al.* Effects of thermal annealing treatment on the optical and the electrical properties of GaN films grown on Si substrates. *J. Korean Phys. Soc.* **60**, 1809–1813 (2012).
87. Fakhri, M. A., Wahid, M. H. A., Abdulwahhab, A. W., Hashim, U. & Salim, Z. T. Efficiency enhancement of optical strip waveguide by the effect of heat treatment. *Optik* **180**, 768–774 (2019).
88. Ismail, R. A. & Fadhil, F. A. Effect of electric field on the properties of bismuth oxide nanoparticles prepared by laser ablation in water. *J. Mater. Sci. Mater. Electron.* **25**, 1435–1440 (2014).
89. Alias, E. A. *et al.* Effect of annealing temperature and ambience on roughened GaN substrate. *Mater. Sci. Semicond. Process.* **148**, 106777 (2022).
90. Salim, E. T., Abdulwahhab, A. W., Hashim, U. & Salim, Z. T. Optical properties of micro and nano LiNbO₃ thin film prepared by spin coating. *Opt. Laser Technol.* **103**, 226–232. <https://doi.org/10.1016/j.optlastec.2018.01.040> (2018).
91. Dubey, A. *et al.* Aluminum plasmonics enriched ultraviolet GaN photodetector with ultrahigh responsivity, detectivity, and broad bandwidth. *Adv. Sci.* **7**(24), 2002274 (2020).
92. Fakhri, M. A., Hashim, U., Abdulwahhab, A. W. & Salim, Z. T. Annealing temperature effect on structural and morphological properties of nano photonic LiNbO₃. *J. Mater. Sci. Mater. Electron.* **28**(22), 16728–16735 (2017).
93. Abdulwahhab, A. W., Kadhim, S. M., Alwazni, M. S. & Adnan, S. A. Thermal oxidation effects on physical properties of CuO₂ thin films for optoelectronic application. *Mater. Res. Express* **6**(2), 026429 (2018).
94. Al-Douri, Y., Bouhemadou, A., Khenata, R. & Ameri, M. Stirrer time effect on optical properties of nanophotonic LiNbO₃. *Mater. Chem. Phys.* **203**, 243–248 (2018).
95. Ismail, R. A., Al-Samarai, A.-M.E., Mohmed, S. J. & Ahmed, H. H. Characteristics of nanostructured CdO/Si heterojunction photodetector synthesized by CBD. *Solid-State Electron.* **82**, 115–121 (2013).
96. Faisal, A. D., Ismail, R. A. & Khalef, W. K. Synthesis of ZnO nanorods on a silicon substrate via hydrothermal route for optoelectronic applications. *Opt. Quantum Electron.* **52**, 1–12 (2020).

97. Aslam, S. *et al.* External quantum efficiency of Pt/n-GaN Schottky diodes in the spectral range 5–500 nm. *Nucl. Instrum. Methods Phys. Res. Sect. A* **539**(1–2), 84–92 (2005).
98. Chen, W. C., Kuo, S. Y., Lai, F. I., Lin, W. T. & Hsiao, C. N. Effect of substrate temperature on structural and optical properties of InN epilayer grown on GaN template. *Thin Solid Films* **529**, 169–172 (2013).
99. Shim, S. K. *et al.* Nanopatterned sapphire substrate to enhance the efficiency of AlGaIn-based UVC light source tube with CNT electron-beam. *J. Mater. Chem. C* **8**, 17336–17341 (2020).
100. Tawfik, W. Z., Hyun, G. Y., Ryu, S.-W., Ha, J. S. & Lee, J. K. Piezoelectric field in highly stressed GaN-based LED on Si (111) substrate. *Opt. Mater.* **55**, 17–21. <https://doi.org/10.1016/j.optmat.2016.03.013> (2016).
101. Abood, M. K., Salim, E. T. & Saimon, J. A. Niobium pentoxide thin film prepared using simple colloidal suspension for optoelectronic application. *Int. J. Nanoelectron. Mater.* **11**(2), 127–134 (2018).
102. Zhang, C. G., Bian, L. F., Chen, W. D. & Hsu, C. C. Effect of growth conditions on the GaN thin film by sputtering deposition. *J. Cryst. Growth* **299**(2), 268–271 (2007).
103. Fakhri, M. A., Wahid, M. H. A., Hashim, U., Salim, Z. T. & Ismail, R. A. Synthesis and characterization of nanostructured LiNbO₃ films with variation of stirring duration. *J. Mater. Sci. Mater. Electron.* **28**(16), 11813–11822 (2017).
104. Jiang, H. H. *et al.* GaN MSM structure UV photodetector detector based on nonplanar Si substrate and its performance optimization. *Semicond. Sci. Technol.* **37**(10), 105020 (2022).

Acknowledgements

The authors would like to thank the University of Technology-Iraq for the logistic support this work. The authors extend their appreciation to the Deanship of Scientific Research at Northern Border University, Arar, KSA for funding this research work through the project number “NBU-FFR-2023-0048. The authors gratefully thank the Prince Faisal bin Khalid bin Sultan Research Chair in Renewable Energy Studies and Applications (PFCRE) at Northern Border University for their support and assistance. The authors would like to thank Al-Farahidi University, Baghdad, Iraq for the logistic support this work.

Author contributions

M.A.F., H.D.J., M.J.A., E.T.S., A.S.A., R.K.I., R.A.I., Conceptualization, M.A.F., H.D.J., M.J.A., E.T.S.; methodology, M.A.F., H.D.J., M.J.A., E.T.S.; validation, M.A.F., E.T.S., A.S.A., R.K.I., R.A.I.; formal analysis, M.A.F., H.D.J., M.J.A., E.T.S.; investigation, M.A.F., H.D.J., E.T.S., A.S.A., R.K.I., R.A.I.; resources, M.A.F., E.T.S., A.S.A., R.K.I., R.A.I.; data curation, M.A.F., H.D.J., E.T.S.; writing—original draft preparation, H.D.J.; writing—review and editing, M.A.F., M.J.A., E.T.S., A.S.A., R.K.I., R.A.I.; visualization, M.A.F., H.D.J., M.J.A., E.T.S., A.S.A., R.K.I., R.A.I.; supervision, M.A.F., M.J.A., project administration, M.A.F., M.J.A., E.T.S., funding acquisition, A.S.A., All authors have read and agreed to the published version of the manuscript.

Funding

The authors extend their appreciation to the Deanship of Scientific Research at Northern Border University, Arar, KSA for funding this research work through the project number “NBU-FFR-2023-0048.

Competing interests

The authors declare no competing interests.

Additional information

Correspondence and requests for materials should be addressed to M.A.F., E.T.S. or A.S.A.

Reprints and permissions information is available at www.nature.com/reprints.

Publisher’s note Springer Nature remains neutral with regard to jurisdictional claims in published maps and institutional affiliations.



Open Access This article is licensed under a Creative Commons Attribution 4.0 International License, which permits use, sharing, adaptation, distribution and reproduction in any medium or format, as long as you give appropriate credit to the original author(s) and the source, provide a link to the Creative Commons licence, and indicate if changes were made. The images or other third party material in this article are included in the article’s Creative Commons licence, unless indicated otherwise in a credit line to the material. If material is not included in the article’s Creative Commons licence and your intended use is not permitted by statutory regulation or exceeds the permitted use, you will need to obtain permission directly from the copyright holder. To view a copy of this licence, visit <http://creativecommons.org/licenses/by/4.0/>.

© The Author(s) 2023